PONTIFICIA UNIVERSIDAD CATOLICA DE CHILE
ESCUELA DE INGENIERÍA

DYNAMIC CHARACTERISTICS OF A LONGITUDINALLY ASYMMETRICAL MULTI-SPAN SUSPENSION BRIDGE: THE CHACAO BRIDGE

DIEGO MARTÍN PIZARRO POHL

Thesis submitted to the Office of Research and Graduate Studies
in partial fulfillment of the requirements for the degree of
Master of Science in Engineering

Advisor:
MATÍAS ANDRÉS HUBE GINESTAR

Santiago de Chile, September 2015

PONTIFICIA UNIVERSIDAD CATOLICA DE CHILE
ESCUELA DE INGENIERÍA

DYNAMIC CHARACTERISTICS OF A LONGITUDINALLY ASYMMETRICAL MULTI-SPAN SUSPENSION BRIDGE: THE CHACAO BRIDGE

DIEGO MARTÍN PIZARRO POHL

Members of the Committee:
MATÍAS ANDRÉS HUBE GINESTAR
DIEGO LÓPEZ-GARCÍA GONZÁLEZ
MATÍAS ANDRÉS VALENZUELA SAAVEDRA
JOSÉ LUIS ALMAZÁN CAMPILLAY

Thesis submitted to the Office of Research and Graduate Studies
in partial fulfillment of the requirements for the degree of
Master of Science in Engineering

Santiago de Chile, September 2015

Gratefully to my sister, mother and father

ACKNOWLEDGEMENTS

I express my deep sense of gratitude to my advisor, Professor Matías Hube Ginestar, for the confidence he had in me, and for all the time he spent advising me, correcting the work and helping me to conduct my thesis. I am very thankful to Matías Valenzuela Saavedra, who gave us the chance to work with the MOP to do research of the Chacao Bridge. He dedicated time on answering our questions, correcting the documents and giving us all the information that we needed, which was fundamental to develop the thesis.

I also want to thank to my friends that helped me during the past two years while I was working in the thesis. Special thanks to those who worked with me in the same office, La Pecera: Sebastián Castro, Gaspar Auad, Mathias Haindl, Ashley Stanton-Yonge, Pablo Iturrieta, Cristóbal Valderrama, Pamela Pérez, Ernesto Ortiz, Claudia Álvarez, Jose Maringue, Mauricio Ferj, Sebastián Calderón, Jose Wilchez and Antonio Marínez, thank you for all those good conversations, lunches and funny moments that we shared inside and outside the office.

Thanks to Alejandro Simonetti, who helped me and my family during the first year of my studies.

I also thank to the Chilean Fondo Nacional de Ciencia y Tecnología (FONDECYT) for their support through grant #11121581, to CONICYT- PCHA/MagisterNacional/2015-22151039, and the National Research Center for Integrated Natural Disaster Management CONICYT/FONDAP/1510017. This study was done under the collaboration agreement between PUC and MOP signed on 01/13/2015 (#8507416)

Finally, thanks my family, specially to my sister and my mother for all the support during my studies, and to my father that has always been with from heaven.

TABLE OF CONTENTS

LIST OF FIGURES

LIST OF TABLES

ABSTRACT

The objective of this research is to study the dynamic characteristics of a longitudinally asymmetrical multi-span suspension bridge. The current design of the Chacao Bridge (as of March 2015) in Chile is considered as a case study. With a total length of 2.75 km and two main spans of 1,155 m and 1,055 m, the Chacao Bridge will be the suspension structure with the longest span in Latin America and the longest multi-span suspension bridge in the world. Since the bridge will be located in a high seismic region, the main objective of this paper is to determine the relevant modes that affect the base shear of the pylons. To achieve this objective, a three dimensional finite element model of the bridge is developed in ANSYS. Before the modal analysis, a static analysis is carried out to establish the equilibrium condition of the bridge due to dead load. Results showed that the first transverse frequency is 0.0625 Hz and the first vertical frequency is 0.1115 Hz. The estimated frequencies and mode shapes are compared with those of a symmetrical multi-span suspension bridge with similar characteristics. The modal contribution for the base shears of the three pylons, and for the longitudinal displacement at the top of the central pylon are obtained using a design spectrum. Finally, a parametric study is conducted to analyze the influence of providing central clamps and of modifying the stiffness of the central pylon, on the seismic response of the bridge.

Keywords: suspension bridge; multi-span; modal contribution; long span; cables

RESUMEN

El objetivo de esta investigación es estudiar las características dinámicas de un puente colgante longitudinalmente asimétrico de múltiples vanos. El diseño actual del Puente Chacao (hasta Marzo de 2015) se utilizará como caso de estudio. Con un largo total de 2.75 km y dos vanos principales de 1,1155 m y 1.055 m, el Puente Chacao será la estructura con el vano más grande de Latino America y el puente colgante de múltiples vanos maás largo del mundo. Como el puente estará localizado en una zona altamente sísmica, el principal objetivo de esta tesis es determinar los modos relevantes que afectan al corte basal de las pilas. Para alcanzar este objetivo, se realizó un modelo tridimensional de elementos finitos, desarrollado en ANSYS. Antes de realizar el análisis modal, se debe correr un análisis estático para establecer la condición de equilibrio del puente bajo cargas muertas. Los resultados muestran que la primera frecuencia transversal del puente es 0.0625 Hz, y la primera vertical es 0.1115 Hz. Las frecuencias y formas modales estimadas se comparan con las de un puente colgante de múltiples vanos simétrico de características similares. La contribución modal al corte basal de las tres pilas, y para el desplazamiento longitudinal de la punta de la pila central se obtuvieron utilizando un espectro de diseño. Finalmente, se realizó un análisis paramétrico para analizar la influencia de agregar abrazaderas centrales y de modificar la rigidez de la pila central en la respuesta sísmica del puente.

Palabras Claves: puente colgante; múltiples vanos; contribución modal; grandes vanos; cables

1. INTRODUCTION

1.1. Motivation

Nowadays, suspension bridges are recognized as the most feasible structural concept for spans exceeding 1,200 m (Forsberg, 2001). As the world is hunger to increase connectivity, the demand for this kind of bridges is increasing, challenging engineers to span longer channels. Several remarkable suspension bridges exist across the world, most of them are located in United States, Denmark, Norway, South Korea, China and Japan, and the construction of these bridges has contributed to the understanding of the dynamic and static behavior of these structures. For example, the George Washington Bridge (1931) and the Golden Gate Bridge (1937) were the first two bridges with a span larger than 1000 m, and the collapse of the Tacoma Narrows Bridge on 1940 helped to understand the wind effect on suspension bridges. One of the most emblematic structures is the Akashi Kaikyo Bridge, built in Japan in 1998. The total length of this bridge is 3,900 m and its main span of 1,991 m holds the world record. The Akashi Kaikyo bridge resisted the Mw = 7.2 Southern Hyogo Earthquake when it was under construction in 1995, which caused permanent displacements of the foundation pylons that changed the initial geometry of the bridge. (Tada, Jin, Kitagawa, Nitta, & Toriumi, 1995)

In Chile the longest suspension bridge is the Presidente Ibañez with a main span of 210 m, and second longest suspension bridge is the bridge Augusto Grosse, with a main span of 138 m. But in 2014 the project of the Chacao Bridge was a awarded to a consortium. This project features a bridge with two main spans of 1055 m and 1155 m, one side span of 284 m and an approach bridge of 140 m long, being by far the longest span in Chile, and even in South America.

The Chacao Bridge is a major challenge for Chile as it will be the first time that a long span suspension bridge will be constructed, and also because the special configuration of the Chacao Bridge, a longitudinally asymmetric multi-span suspension bridge. For theses reasons, reasons that the Ministry of Public Works (MOP), the institution in charge of

Figure 1.1. Presidente Ibañez Bridge

the Chacao Bridge, wants to transmit all the technology and knowledge of this project to Chilean engineers. On this context, the Ministry of Public Works and the Pontificia Universidad Católica signed a collaboration agreement, which main objective is to produce research about the Chacao Bridge on topics of interest to both parts.

1.2. State of the art

1.2.1. Suspension Bridges

In the family of bridge systems, the cable supported bridges are distinguished by their ability to overcome large spans. At present, cable supported bridges are enabled for spans in the range from 200 m to more than 2000 m (Gimsing & Georgakis, 2012). There are two main types of cable supported bridges, characterized by the configuration of the cable system: the cable-stayed system (Figure 1.2(a)), which contains straight cables connecting the deck to the pylons, and the suspension system (Figure 1.2(b)), that comprises a parabolic main cable and vertical hanger cable connecting the deck to the main cable. While the first system is more efficient in a range of 150 m to 600 m of main span, the second cover the range of 500 m to 2100 m as shown in Figure 1.3 (Abdel-Ghaffar & Nazmy,

1991). This thesis is focused in suspension bridges, and the top 10 longest span bridges in the world are summarized in Table 1.1.

Figure 1.2. (a) Normandy Bridge; (b) Golden Gate Bridge

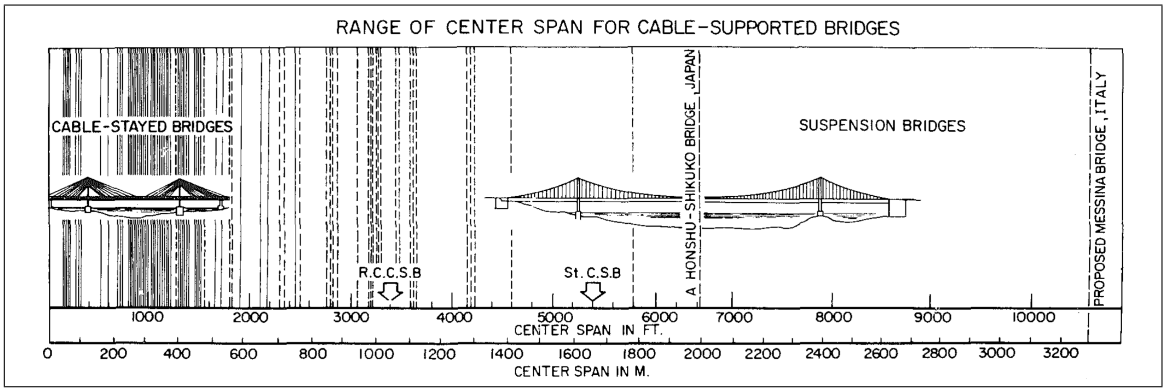

Figure 1.3. Practical range of center or effective span for cable-supported bridges; Each vertical line represents an existing bridge (until 1991)

The main components of the structural system of a cable supported bridge are (Gimsing & Georgakis, 2012):

- Deck or stiffening girder: Structural element subjected to the major part of the external load, because the total traffic load is applied directly to it. Also, in most bridge the dead load and the wind area are larger for the deck than for the cable system.
- Cable system: Its main function is to carry the loads from the deck to the pylons. In suspension bridges, it is formed by the main cable and the hangers.

Table 1.1. Top 10 longest-span bridges in the world (until 2015)

No	Name	Main Span [m]	Country	Year Built
1	Akashi Kaikyo	1991	Japan	1998
2	Xihoumen	1650	China	2009
3	Great Belt	1624	Denmark	1998
4	Yi Sun-sin	1545	South Korea	2012
5	Runyang	1490	China	2005
6	Nanjing Fourth Yangtze	1418	China	2012
7	Humber	1410	United Kingdom	1981
8	Jiangyin	1385	China	1999
9	Tsing Ma	1377	China - Hong Kong	1997
10	Hardanger	1310	Norway	2013

- Pylons: Tower structures that transfers the load from the bridge to the foundations. The most decisive factor on a regular pylon is the axial force originated from the vertical components of the forces in the cables attached to the pylon.
- Anchor blocks: elements that transfers the load from the main cable to the soil.

The described elements of suspension bridges are shown in Figure 1.4. In response to a load in the deck, the load transfer should follow this sequence: from the deck to the hangers, then to the main cables until the pylons and the anchor blocks, where the load is carried to the ground.

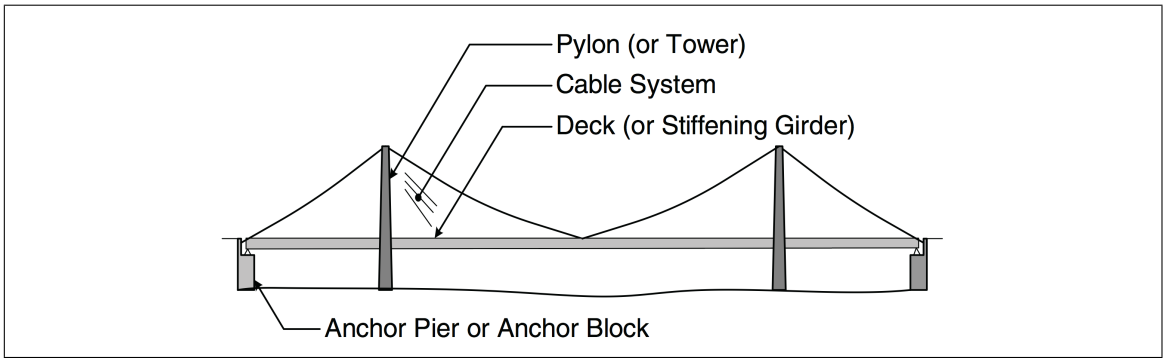

Figure 1.4. Main components of a cable supported bridge (Gimsing & Gerogakis, 2012)

An effective finite element model to obtain the dynamic characteristics of a suspension bridge is known as “fish spine” or “backbone” model. The pylons are represented with beam elements, the main cables and hangers with cable or truss (only tension) elements, and for the deck special considerations must be taken. Since the sectional properties of the bridge deck rather than its structural details affect the natural frequencies of the bridge, the deck in the fish spine model is commonly represented by a single equivalent beam (Xu, Ko, & Zhang, 1997). The connection between the deck and the hangers is achieved with rigid arms. An example of this type of model is shown in Figure 1.5.

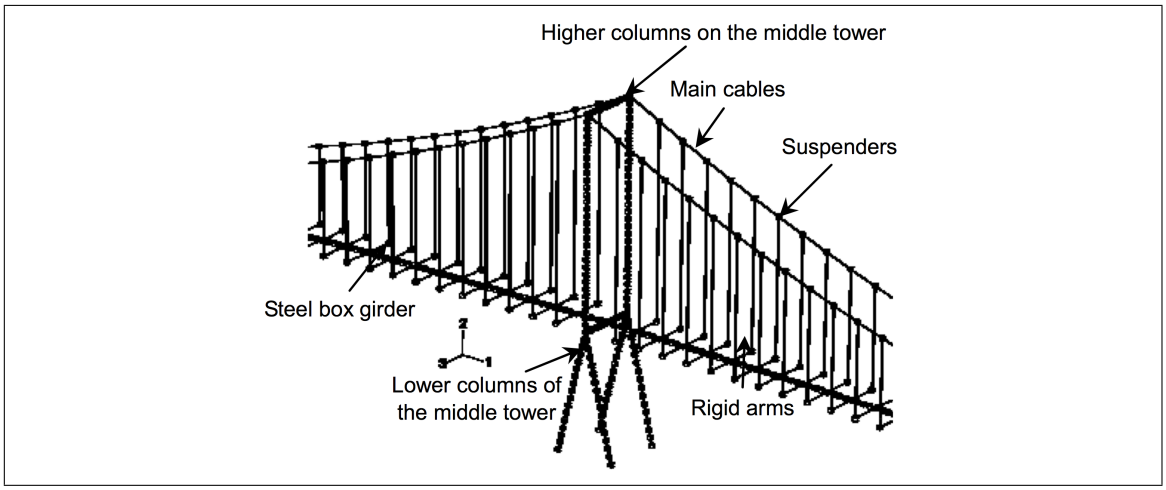

Figure 1.5. Fish spine model of a bridge

Using the described model, Xu et al (1997) made vibration studies of the Tsing Ma Suspension Bridge. The bridge has 206 m height pylons, one main span of 1377 m, one side span of 455 m and the other one with 300 m. He made a modal analysis with a finite element model developed with DDJ-W software. The dynamic characteristics of the bridge are shown in Table 1.2 and Table 1.3. It must be noticed that on the first and second lateral modes (Fig 1.6), the movement of the two main span cables and deck is in phase, while in the third and fourth ones, the cables and decks are out of phase as the deck exhibited almost no movement.

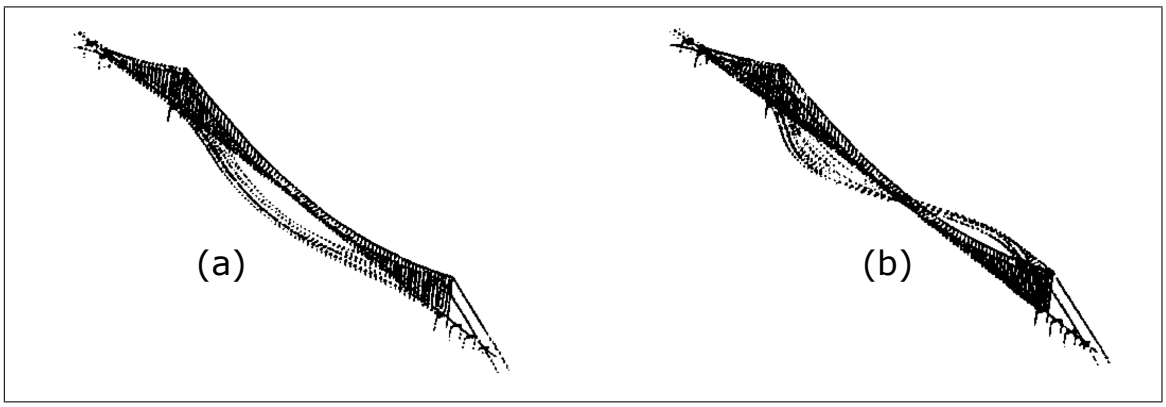

Figure 1.6. Lateral modes of Tsing Ma Bridge (a) First; (b) Second (Xu et al, 1997)

Table 1.2. Characteristics of lateral modes of the Tsing Ma Bridge

Order number	Period (s)	Characteristic of modes
1	14.7059	Symmetric lateral vibration of the main cables and the deck (half wave)
2	6.3219	Antisymmetric lateral vibration of the main cables and the deck (one wave)
3	4.7619	Symmetric lateral vibration of the main cables (half wave)
4	4.3478	Antisymmetric lateral vibration of the main cables (one wave)

Table 1.3. Characteristics of vertical modes of the Tsing Ma Bridge

Number	Period (s)	Characteristic of modes
1	8.5470	Antisymmetric vertical vibration of the main cables and the deck (one wave)
2	7.2993	Symmetric vertical vibration of the main cables and the deck (half wave)
3	5.2910	Symmetric vertical vibration of the main cables and the deck (3/2 wave)
4	4.0816	Antisymmetric vertical vibration of the main cables (2 waves)

The seismic behavior and dynamic characteristics of suspension bridges have been widely studied. Irvine (H. Irvine, 1980) studied the earthquake-generated increase in the tension of the main cables with a response spectrum approach and Abdel-Ghaffar & Rubin (Abdel-Ghafar & Rubin, 1983) presented an analytical method for estimating vertical seismic behavior of bridges. Regarding the dynamic characteristics, Abdel-Rohman (Abdel-Rohman, 2010) showed that higher order modes of a suspension bridge have a

large influence on the dynamic response, and Siringorino & Fujino (Siringoringo & Fujino, 2008) conducted a system identification of three long-span bridges using seismic records obtained in Japan.

1.2.2. Multi-Span Suspension Bridges

Most suspension bridges are designed with two pylons and one, two or three suspension spans. However, local conditions might favor the construction of suspension bridges with more than three consecutive spans (Gimsing & Georgakis, 2012). This latter bridges are called multi-span suspension bridges and they have more than one main spans, two side spans, and one anchors blocks at each end (Ge & Xiang, 2011). Some examples are the Konaruto Bridge (1961) in Japan, with two main spans of 160 m and the Tete Bridge (1973) in Mozambique, with a span arrangement of 90+3x180+90 m. However, China have been leading the construction of multi-span suspension bridges during the last years with the construction of the Taizhou Bridge (Figure 1.7) and Anhui Maanshan Bridge (Figure 1.8). These bridges are characterized by having two main spans of 1,080 m long.

The firsts studies on multi-span suspension bridges started with the design of the San Francisco - Oakland Bay Bridge (1930) in San Francisco, CA. Two designs were proposed (Figure 1.9), a multi-span suspension bridge with two main spans of 1,036 m and lateral spans of 393 m, and two consecutive bridges with a central span of 701 m and lateral spans of 352 m (Gimsing & Georgakis, 2012) . The problem with the multi-span option was that when the bridge was subjected to traffic load in only one of the main spans, the deck presented large deflections and the top of the central pylon suffered large horizontal displacements. Due to the high flexibility of the bridge, the multi-span suspension system was discarded, and the two consecutive bridges were constructed.

Other static analysis have been conducted to multi-span suspension bridges. Fukuda (1967) analyzed tentative designs of multi-span suspension bridges to cross the Inland Sea of Japan. He developed a procedure based on the deflection theory and concluded that a central pylon with an A-shape could reduce the deflections of the bridge due to its large

Figure 1.7. Taizhou Bridge (2012)

Figure 1.8. Anhui Maanshan Bridge (2013)

stiffness. Fukuda studied multi-span suspension bridges under lateral (1968) and torsional loads (1975). Sato (1971) also presented a procedure to estimate the deflection in multi-span bridges, but he considered the deflection of the towers in the analysis. Nazir (1986) showed the advantages of a multi-span suspension bridge by estimating the costs of multiple bridge designs using basic cable theory. He focused on how to balance the forces on the central pylon when the bridge is fully loaded in one span. More recently, Thai & Choi (2013) proposed an advanced analysis of multi-span suspension bridges that considers material non-linearities and includes catenary cable elements. With this methodology they predicted the ultimate strength of multi-span suspension bridges for different static load cases.

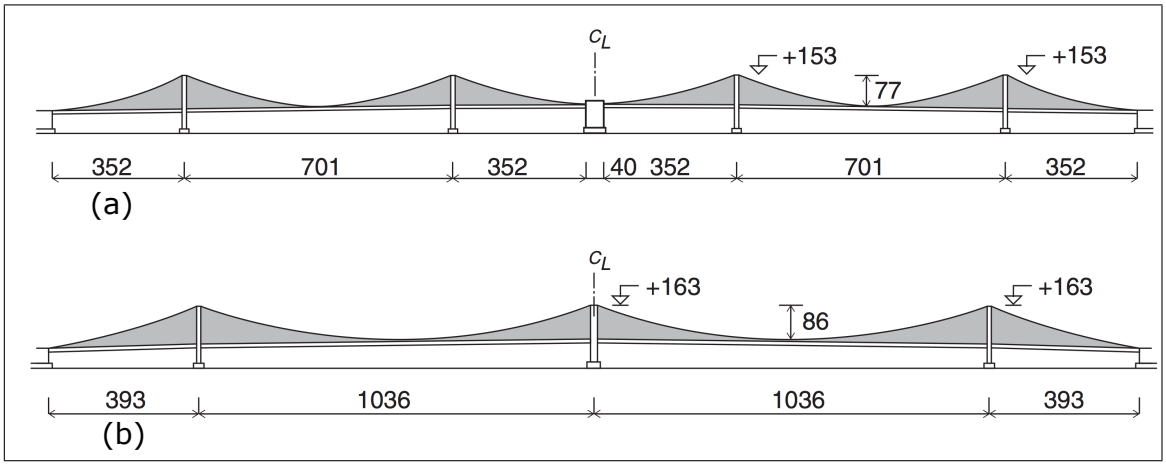

Figure 1.9. San Francisco - Oakland Bay Bridge (a) final design (b) initial design

The authors mentioned above suggest that one of the most important element in multi-span suspension bridges is the central pylon. It stiffness controls the internal forces in the main cables and anchor blocks, and it influences the behavior of the whole bridge when subjected to static and dynamic loads (Yoshida, Okuda, & Moriya, 2004). For gravity loads, the central pylon has to be designed for the most unfavorable load case, which is when full traffic load is applied only in one of the main spans (Gimsing & Georgakis, 2012). as shown in Figure 1.10. Ge et al. (2011) indicates the most important parameters on the design of the central pylon under this critical load. The main parameter to control the design of the central pylon is the longitudinal stiffness, defined in Equation 1.1.

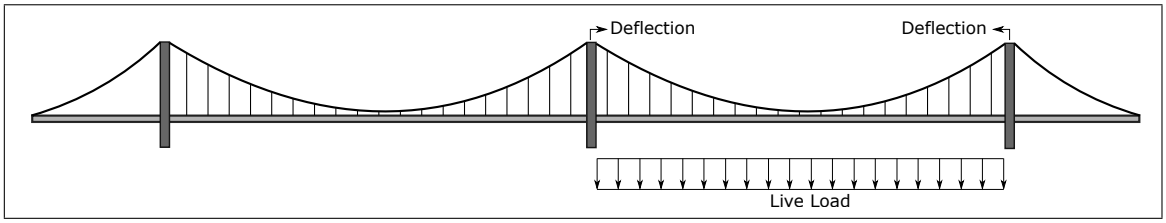

Figure 1.10. Critical load for multi-span bridges

$$R_b = \frac{|T_1 \cos(\alpha_1) - T_2 \cos(\alpha_2)|}{\delta_b} \tag{1.1}$$

Where T_1 and T_2 are the forces in the cables at the central pylon top, α_1 and α_2 are the angles of the cables at the top of the central pylon, and δ_b the longitudinal displacement of the central pylon top. This longitudinal stiffness controls the bridge performance, but the selection of R_b must be carefully selected by checking four important factors:

1) δ_d = Vertical deflection of the deck, which increases if R_b is decreased
2) δ_b = Longitudinal displacement of the top of the central pylon, which increases if R_b is decreased
3) σ_m = maximum and minimum stress in the legs of the central pylon, which increases if R_b is increased
4) K_s = safety factor of sliding resistance, which decreases if R_b is increased. The safety factor is defined as:

$$K_s = \frac{\mu\theta}{\ln(T_1/T_2)} \tag{1.2}$$

Where μ is the friction factor between the main cable and saddle pad (selected as 0.2 based on experiments), T_1 and T_2 are the tension forces ($T_1 > T_2$), and θ is the angle of the saddle arc (Figure 1.11). The slip resistance of the main cable on the middle tower saddle is very important, because the force difference in the main cable at both sides of the central pylon is large when the critical load for multi-span bridges is applied (Qiang, He-qiang, & Guang-wu, 2012). For example, for the Anhui Maanshan Bridge and Taizhou Bridge in China the minimum value for the safety factor of sliding resistance is 2 ($K_s \geq 2$).

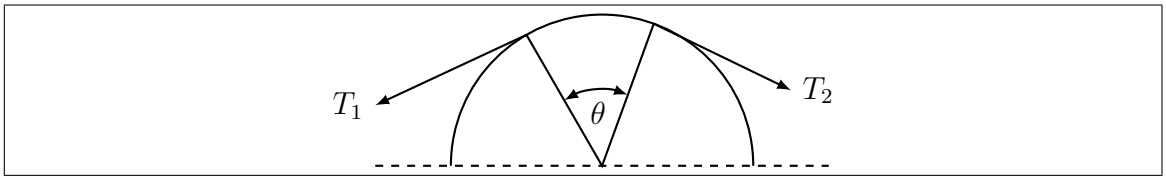

Figure 1.11. Angle of the saddle arc

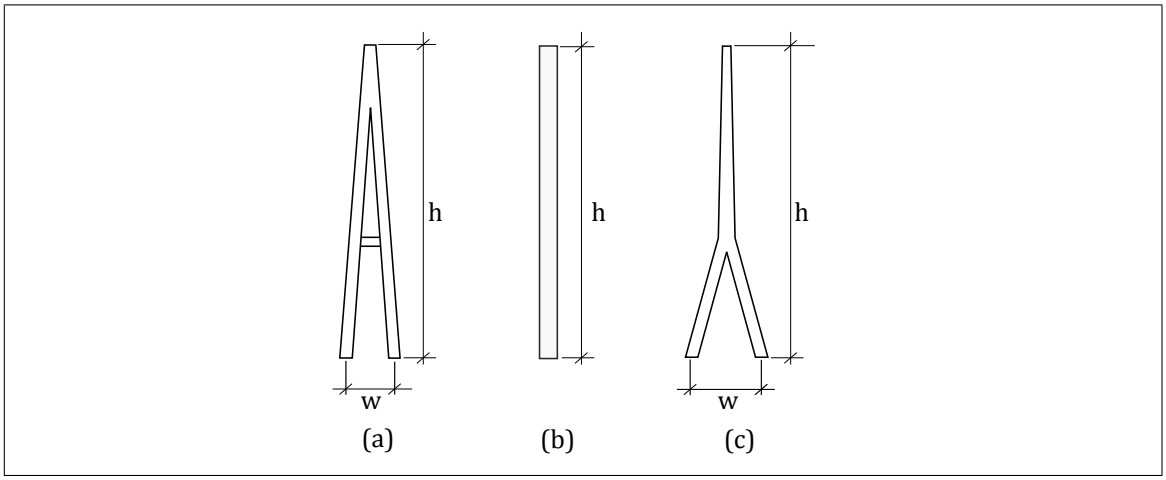

Figure 1.12. Longitudinal shape of central pylon (a) A-shaped; (b) I-shaped and; (c) Inverted Y-shaped (Ge et al. 2011)

Three types of central pylons have been proposed. The A-shaped pylon (Figure 1.12 (a)), which has a relatively large longitudinal stiffness. With this pylon, the vertical displacement at the mid-span deck and the longitudinal displacement at the central pylon top are relatively small, but the safety factor of sliding resistance and stresses in the legs of the pylons are unfavorable. The I-shaped pylon (Figure 1.12 (c)) has a low longitudinal stiffness, but favorable stresses and safety factor. The third type of pylon is the inverted Y-shaped pylon (Figure 1.12(b)), which is a combination of the two shapes mentioned above. Ge (2011) showed an interesting analysis of how the central pylon of the Taizhou Bridge was selected. The considered pylon was an inverted Y-shape, which was the main innovation on this kind of bridges (Figure 1.13). Qiang (2012) shows how the I-shaped central pylon of the Anhui Maanshan Bridge was selected (Figure 1.14).

The dynamic characteristics and behavior of multi-span suspension bridges have also been studied by several authors. Ge & Xiang (2011) made a comparison of the modal frequencies between multi-span and classic suspension bridges using the geometry of the Maanshan Bridge and a classic suspension bridge with a span of 2,160 m. They obtained that the frequency of the first mode of the multi-span suspension bridge was 2.5 times larger than that of the classical bridge. Wang et al. (2014) described the dynamic characteristics of the Taizhou Bridge and conducted a parametric study on flutter stability of

Figure 1.13. Construction of the Y-shape central pylon of the Taizhou Bridge

the bridge by using a finite element model in ANSYS. For the parametric study, they varied the vertical and torsional stiffness of the deck and the stiffness of the central pylon, concluding that the parameters of the deck have larger influence on flutter stability than the stiffness of the central pylon. Zhang & Ge (2014) conducted a full aeroelastic model testing of the Maanshan Bridge to evaluate the flutter performance. They identified a flutter-mode transition in a smooth wind flow, a phenomenon that was observed only at that bridge. Regarding seismic behavior, Li et al. (2014) conducted a shaking table test of the Taizhou Bridge using a 1/40 scale model. They incorporated viscous dampers between the central pylon and the deck, concluding that the viscous dampers decreased effectively the longitudinal relative displacement between the deck and the central pylon.

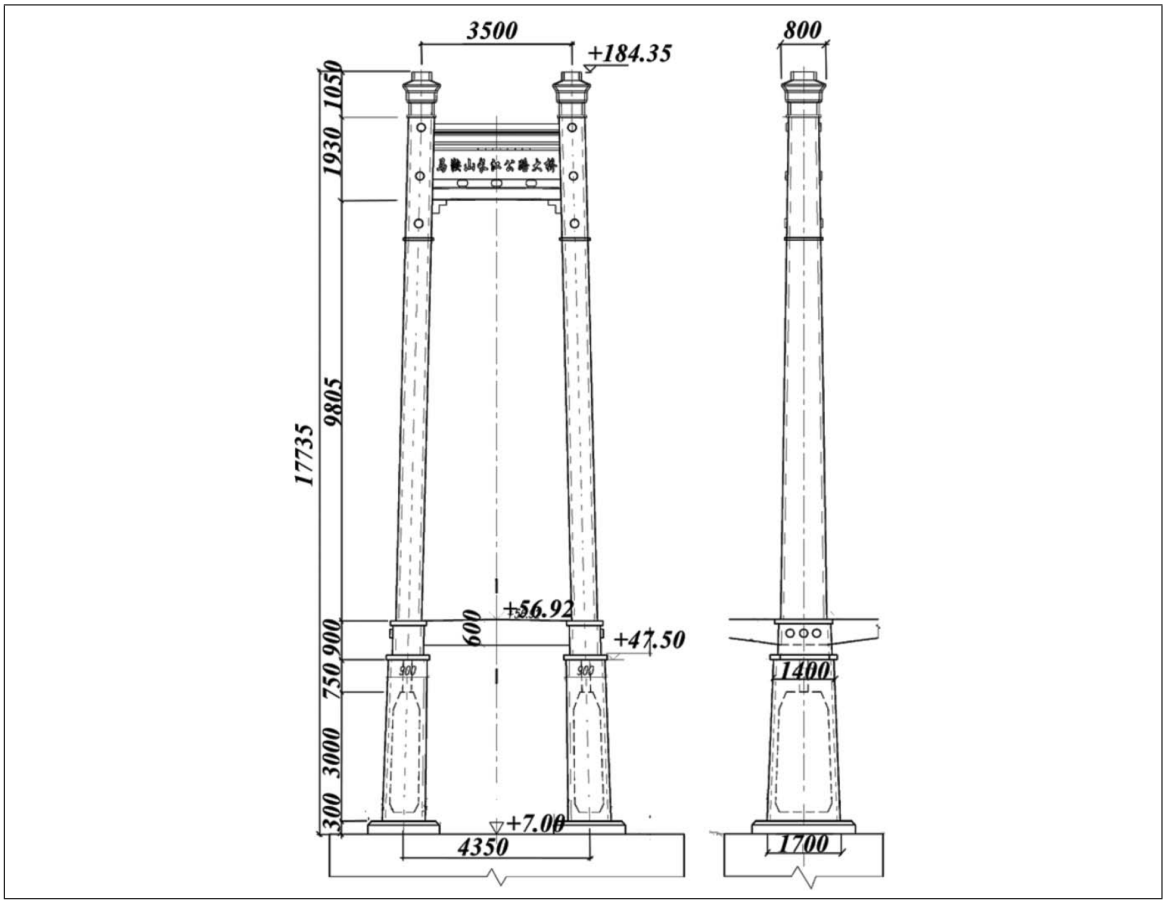

Figure 1.14. I-shape central pylon of the Anhui Maanshan Bridge (Ge et al, 2011)

1.3. Objectives

The bridges of the referred studies are longitudinally symmetrical, and no studies have been conducted for multi-span bridges with longitudinal asymmetry. In this research, the dynamic characteristics of longitudinally asymmetrical multi-span bridges are studied. The preliminary design of the Chacao Bridge (as in March 2015) is selected, a multi-span suspension bridge that will be constructed in Chile, a highly seismic country, and that has a longitudinal asymmetrical configuration. The first objective of this study is to obtain the dynamic characteristics of the Chacao Bridge. The second objective is to determine which are the relevant modes that affect the base shear of the pylons. This objective is relevant because long-span bridges modes have very large periods (larger than 10 seconds) and

seismic design spectrums are usually well defined for structures with fundamental period less than 3.5 seconds. Therefore, it is of great interest to understand if spectral ordinates for long periods are relevant for the base shear. The third objective is to study the effect of the inclusion of central clamps between the main cables and deck, and the effect of the stiffness of the central pylon on the seismic behavior of the bridge and on the seismic base shear.

1.4. Thesis structure

In Chapter 1, Introduction, the motivation of the work, the state of the art of multi-span suspension bridges and the objectives of the thesis are presented.

Chapter 2 describes the cable element will be explained, starting from the basic static equations to the dynamic behavior. The last part of this chapter focuses in the cable modeling in ANSYS.

The Chacao Bridge is presented in Chapter 3. The details and dimensions of the Chacao Bridge that will be used to develop the finite element model are described. A brief history of the bridge is also presented.

The Finite Element Model of the bridge is described in Chapter 4. The elements, materials, sections, boundary conditions and the analysis of the selected prestrain for the main cables is presented.

In Chapter 5, the frequencies and mode shapes of the bridge are shown and described. They are also compared with those of a longitudinally symmetric multi-span suspension bridge. The modal contribution factors to the base shear of the pylons are summarized and analyzed, and the longitudinal displacement of the top of the central pylon is calculated.

Chapter 6 describes the parametric analysis. Central clamps are included in the model to appreciate their effects in the base shear. Three cases are evaluate: central clamps in the north span, in the south span and in both spans at the same time. The second parameter

that was varied is the stiffness of the central pylon. In both analysis the base shear and longitudinal displacement of the central pylon is analyzed.

Finally, the conclusions of this thesis and future works are presented in Chapter 7.

2. CABLES

Cables are a very important element in suspension bridges, and the choice of the cable system is probably the most decisive factor in the design of suspension bridges (Gimsing & Georgakis, 2012). They transfer the traffic load of the self-weight of the deck and the dead loads to the pylon and they also have a significant influence on the dynamic characteristics of the bridge. For that purpose, it is important to understand the behavior of cables and how they can be modeled. This chapter focuses in the static and dynamic behavior of cables, starting from the basic formulas of cables under uniformly distributed forces and cables under its self-weight.

2.1. Equation of state for a 2D cable subjected to vertical load

Considering the cable and coordinates shown in Figure 2.1 subjected to a distributed vertical load $w(x)$, the cable curve A-B is determined by the equation (Gimsing & Georgakis, 2012):

$$y(x) = -\frac{M(x)}{H} + \frac{h}{a} \cdot x \tag{2.1}$$

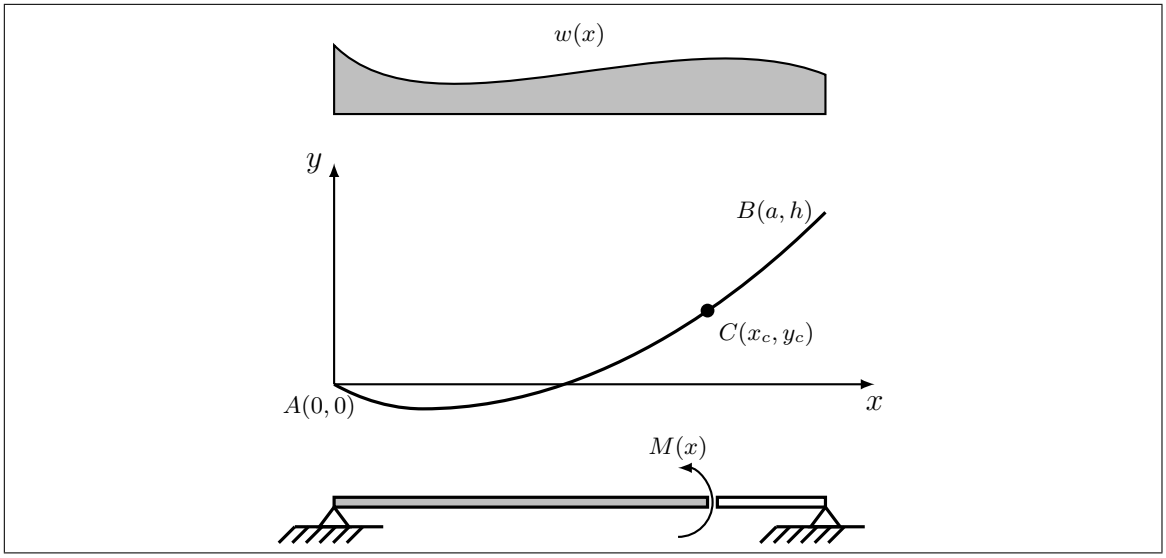

Figure 2.1. Cable under vertical load $w(x)$

Where $M(x)$ is the bending moment of the simple supported beam with the same span and load as the cable and H is the magnitude of the horizontal force of the cable. The cable configuration can be determined by one of three conditions: the horizontal force H, the position of a third point C on the cable or the total length of the cable. If the position the point C is known, H can be obtained by Equation 2.2, and if the length is known, by Equation 2.3.

$$H = \frac{M(x_c)}{hx_c/a - y_c} \tag{2.2}$$

$$s = \int_0^a \sqrt{1 + \left(\frac{dy}{dx}\right)^2} = \int_0^a \sqrt{1 + \left(\frac{h}{a} - \frac{1}{H}\frac{dM}{dx}\right)^2} \tag{2.3}$$

In the case of a multi-span suspension bridge, with a cable system shown in Figure 2.2, the geometry can be expressed by the following equations, based on Equation 2.1:

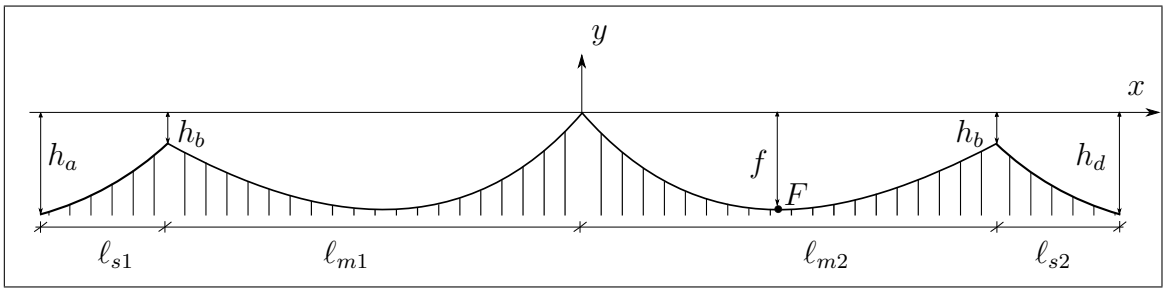

Figure 2.2. Multi span suspension bridge cable system

$$y(x) = \begin{cases} -\dfrac{M_{s1}(x)}{H} - \dfrac{h_b - h_a}{\ell_{s1}}(x + \ell_{m1}) - h_b & \text{if } x > -\ell_{m1} \\ -\dfrac{M_{m1}(x)}{H} + \dfrac{h_b}{\ell_{m1}}x & \text{if } -\ell_{m1} < x < 0 \\ -\dfrac{M_{m2}(x)}{H} - \dfrac{h_c}{\ell_{m2}}x & \text{if } 0 < x < \ell_{m2} \\ -\dfrac{M_{s2}(x)}{H} - \dfrac{h_c - h_d}{\ell_{s2}}(x - \ell_{m2}) - h_c & \text{if } x < \ell_{m2} \end{cases} \tag{2.4}$$

Where $M_{s1}(x), M_{s2}(x), M_{m1}(x)$ and $M_{m2}(x)$ are the moments of simply supported beam with lenghts $\ell_{s1}, \ell_{s2}, \ell_{m1}$ and ℓ_{m2}. If the position of the point F is known, the horizontal tension can be calculated with 2.2, but if the central and side pylon have the same (or similar) height, and the bridge is subjected to a constant distributed load w, the tension

can be obtained by Equation 2.5 (Yoshida et al., 2004)

$$H = \frac{w\ell_{m2}^2}{8f} \tag{2.5}$$

Where f is the maximum sag of the cable. Equations 2.4 and 2.5 are very important as they can give a first approximation to the shape and tension of the main cable of a suspension bridge. If the pylons don't have the same height, Equation 2.5 gives a good first approximation of the horizontal tension of the main cable.

2.2. Stay cable under varying chord force

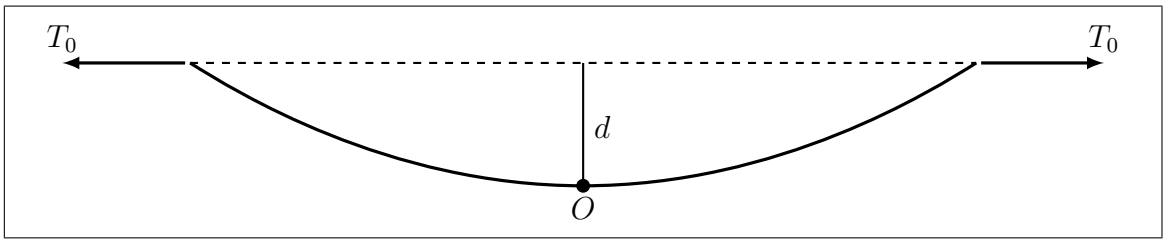

Figure 2.3. Stay cable with chord force T_0 and sag d

Considering an uniform cable suspended from two points and hanging under the action of its self-weight only (Figure 2.3), the cable geometry can determined by the equation (Meriam & Kraige, 2006):

$$y = \frac{T_0}{\mu}\left(\cosh\frac{\mu x}{T_0} - 1\right) \tag{2.6}$$

Where T_0 is the horizontal tension of the cable, μ is the weight per unit of its length and O (Figure 2.3) is the origin of the coordinate system.

2.3. Dynamic behaviour of cables

The equations for in-plane motion for a flat-sag suspended cable anchored on supports at the same level are (M. Irvine, 1981):

$$H\frac{\partial^2 w}{\partial x^2} + h\frac{d^2 z}{dx^2} = m\frac{\partial^2 w}{\partial t^2} \tag{2.7}$$

And for out of plane motion (sway vibration):

$$H\frac{\partial^2 v}{\partial x^2} = m\frac{\partial^2 v}{\partial t^2} \tag{2.8}$$

Where H is the static tensile force, m is the mass per unit length, $v(x,t)$ and $w(x,t)$ are the out of plane and vertical in-plane motion of the cable as a function of time and spatial coordinate (Figure2.4), and h is the time varying part of the cable force:

$$h = \frac{EA}{L_e}\frac{mg}{H}\int_0^{\ell} w dx \tag{2.9}$$

Where ℓ is the horizontal distance between the supports, and $L_e = \int_0^{\ell}(ds/dx)^3 dx \approx \ell(1+8(d/\ell))^2$, a quantity usually a little greater than the span itself, i.e., $L_e \approx \ell$.

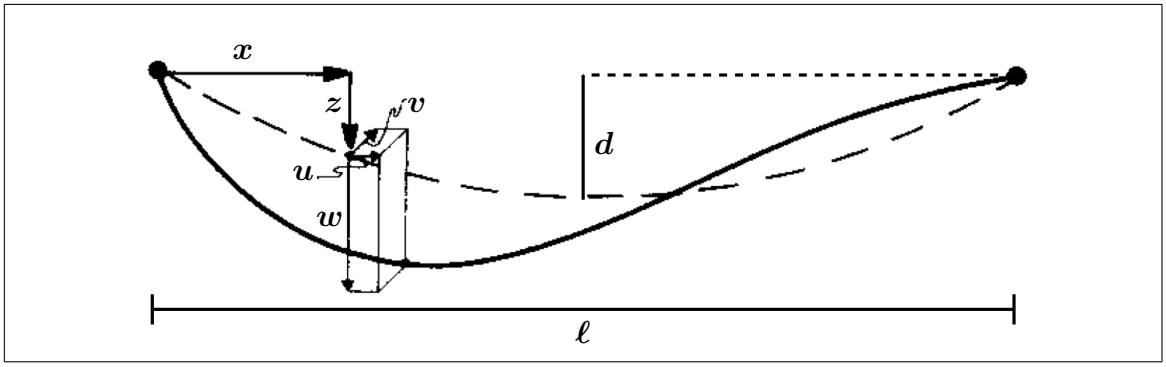

Figure 2.4. Definition diagram showing components of displacement in disturbed profile (Irvine 1981)

From Equation 2.8, the natural frequencies of the sway vibration can be obtained, and are determined by:

$$\omega_n = n\frac{\pi}{\ell}\sqrt{\frac{H}{m}} \tag{2.10}$$

Thus the sway vibration of the sagging horizontal cable with a horizontal force H shows the same natural frequencies as the taut string with a tension $T = H$ (Gimsing & Georgakis, 2012).

For the in plane motion, we can recognize two types of modes: symmetric and anti-symmetric. The asymmetric modes are easy to find because $h = 0$ (because the integral

of the deflection, $\int w dx$, is equal to 0 when the deflection has an asymmetric shape), so the natural frequencies are:

$$\omega_n = n\frac{2\pi}{\ell}\sqrt{\frac{H}{m}} \tag{2.11}$$

In the symmetric modes, $h \neq 0$ and a more complex calculation is required. The natural frequencies can be obtained by solving the following equation:

$$\tan\left(\frac{1}{2}\beta\ell\right) = \left(\frac{1}{2}\beta\ell\right) - \frac{4}{\lambda^2}\left(\frac{1}{2}\beta\ell\right)^3 \tag{2.12}$$

Where β is a parameter involving the natural frequency (Equation 2.13), and λ is a characteristic geometric and elastic parameter that governs the dynamic behaviour of the cable (Equation2.14).

$$\beta^2 = \frac{m\omega^2}{H} \tag{2.13}$$

$$\lambda^2 = \left(\frac{8d}{\ell}\right)^3 \frac{EA}{\mu\ell} \tag{2.14}$$

There are two limit cases for Equation 2.12: when $\lambda^2 \rightarrow \infty$ the cable is inextensible, and the last term of Equation 2.12 can be neglected (the solution of the first four frequencies are shown in Figure 2.5). On the other side, when λ^2 is small, the cable profile approaches a profile of a taut string, and the frequencies are given by Equation 2.10.

Figure 2.5 shows the shape of the first 4 modes of an inextensible sagging cable. It is important to notice that the first mode is asymmetric, while in the case of a taut string the first one is symmetric.

2.4. Cable Modeling

As cables have a highly non linear behavior, the conventional linear analysis which assumes small elastic deformations and displacements is often not applicable. The problem of analyzing cables under different configurations and loading conditions is very complex,

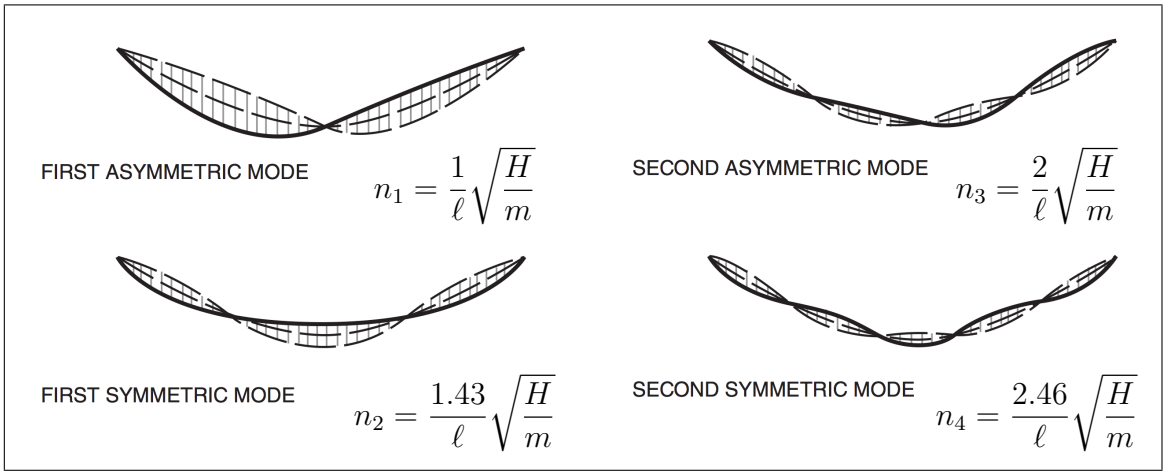

Figure 2.5. Modes of in-plane vibration for the sagging cable (Gimsing 2012)

because stress/strain relationships for cables are highly nonlinear and also large displacements introduce nonlinearities in the geometric sense (Karoumi, 1999).

One of the most used non-linear approach to model cable elements, usually used in cable-stayed bridges, is to consider an only tension truss element with an equivalent tangential modulus of elasticity proposed by Ernst (1965), and the demonstration is showed by Gimsing (2012):

$$E_{eq} = \frac{E}{1 + \frac{(\gamma L_x)^2}{12\sigma^3}E} \tag{2.15}$$

Where E is the material modulus of elasticity, γ is the specific weight of the cable, L_x is the horizontal proyected length of the cable (Figure2.6), and $\sigma = H/A$ is the axial tension in the cable (H the horizontal force in the cable and A the cross section of the cable). It can be noticed that the axial stiffness of the cable is affected by the tension forces (or sag). The net effect is that when the cable tension increases, the sag decreases, and the apparent axial stiffness of the cable increases. The equivalent modulus approach accounts for sag effect, but does not account for the stiffening effect due to large displacements (Ali & Abdel-Ghaffar, 1995).

There are also other authors that had proposed elements with stiffness matrix for this purpose. For example, Karoumi (1999) presents a 2D catenary cable element obtained by

the flexibility method, with the fours degrees of freedom shown in Figure2.6, and Thai (2011) proposed an extrapolated 3D formulation with 6 DOFs. In both cases an iterative Newton-Raphson procedure is necessary to achieve the equilibrium of the system.

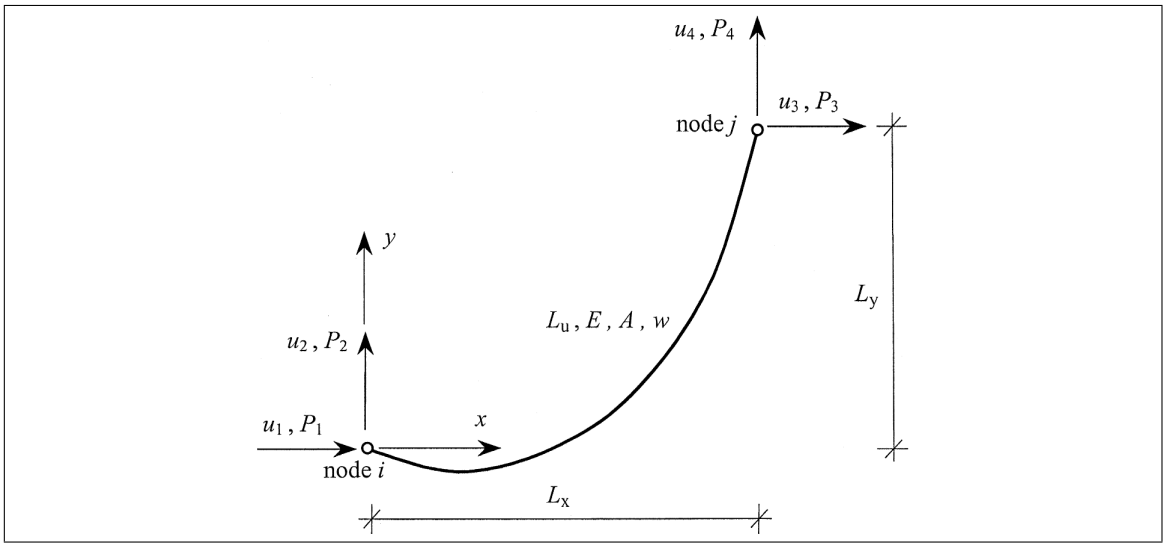

Figure 2.6. Catenary cable element proposed by Karoumi (1999)

2.4.1. Initial configuration

In the design stage of a framed structure such as a beam or a frame, the undeformed configuration of a structure is predetermined based on functional requirements, engineers experiences, etc. The displacement field under dead loads is easily calculated by usual structural analysis techniques based on the predefined undeformed configuration as shown in Figure 2.7 (a). This is because the framed structures posses an initial stiffness independent of applied loads. In the case of a cable structure, however, there is not an unique undeformed configuration corresponding to the equilibrium configuration under dead loads shown in Figure 2.7 (b) because the lateral stiffness of a cable is developed from applied tensions. This is the the most distinctive mechanical property of cable structures. Even though when a cable is loaded by its own self-weight without any external load, a proper tension should be applied to the cable to support the self-weight with a desired shape (Kim & Lee, 2001).

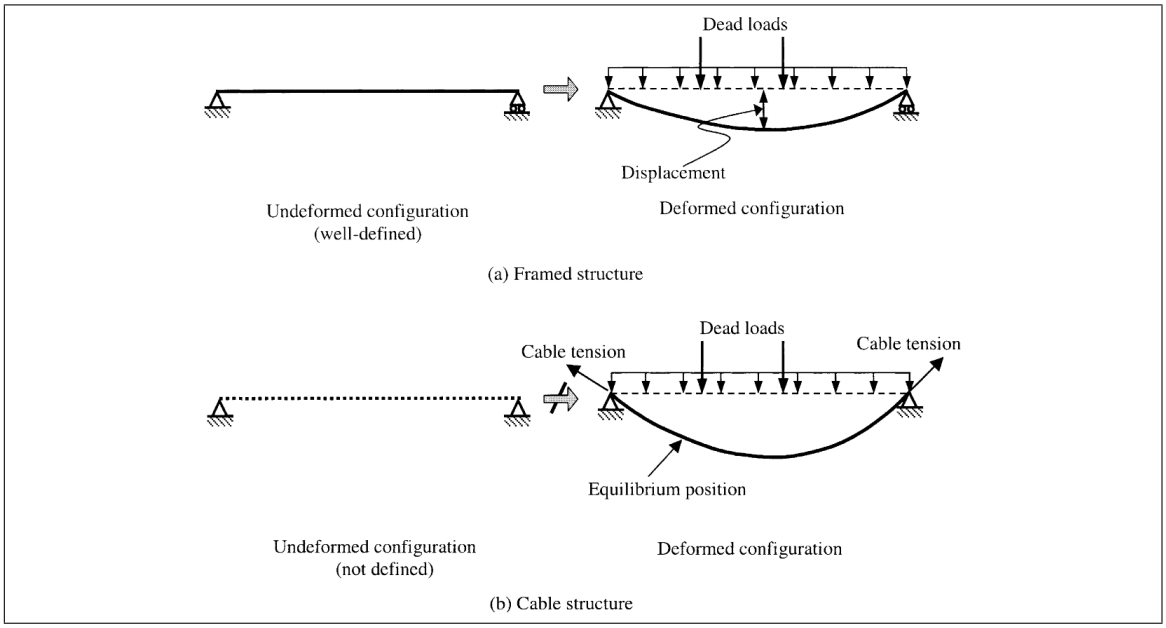

Figure 2.7. Undeformed and deformed configuration (Kim & Lee, 2001)

Usually, the analysis of cable structures, such as bridges, starts with a target configuration under dead loads (TCUD), which is also known as the dead load deformed state or the initial equilibrium configuration. That means that the engineers define some properties of the structure, like the shape of the cable or the main sag based on their experience. But the problem is that they don't know the initial deformed configuration nor the initial tension of the cable (Figure 2.8).

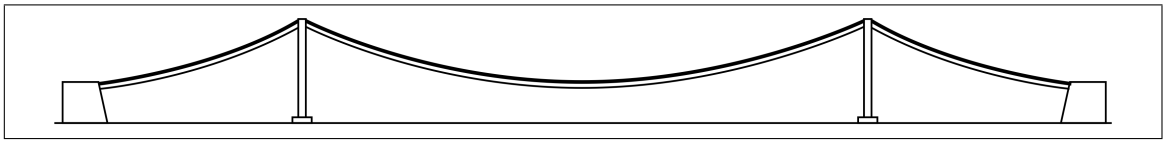

Figure 2.8. Initial configuration of a cable on a suspension bridge (Gimsing & Georgakis, 2012)

There are some methods that help to find the initial tension and shape of the cable under its self-weight. One of them is the trial and error method (Karoumi, 1999), that consist on estimating the initial length or tension of the cable, run a static the analysis, and then, the obtained geometry of the cable must be compared with the target configuration.

If the desired final geometry is not obtained, the process must be repeated with improved values. Kim (2001) shows a rigorous approach, consisting on removing the hangers to analyze the deck and then the main cable by an incremental equilibrium equation using the Newton-Rapshon iteration method.

2.5. Modeling cable elements in ANSYS

Cable elements can be modeled as a tension only truss element using LINK180 elements. It is a 3D spar, also used to model trusses, links, springs, gap, etc (ANSYS® Academic Research, Release 15.0, 2013). By selecting the tension only key-option, the element losses its stiffness if it goes into compression. This element needs an iterative solver, so large-deflection effects (non linear geometry) must be activated in order to use the Newton-Rapshon method. An important input for the LINK180 elements is the initial strain, necessary to calculate the initial stiffness matrix for the first iteration.

On cable structures, only the final geometry due to dead loading is known. An analysis to determine the initial position of the main cables could be done (Figure 2.8), but as the construction of the bridge is sequential and it affects the deflections of the cables, the analysis should consider the construction piece by piece of the deck from the main cables. To avoid this procedure, the analysis should start from the dead load configuration. The method selected is the one explained by Ren (2004). The main idea of the process is that the ideal finite element model of a suspension bridge should be such that on application of the dead load, the geometry of the bridge does not change, since this the input geometry is indeed the equilibrium geometry of the bridge. This can be achieved by manipulating by trial and error the initial tension of the main cables, that in ANSYS must be specified as an input prestrain in the cable elements, and running a static analysis with non linear geometry until a prestrain value that leads to minimum deck deflections is found (Figure 2.9)

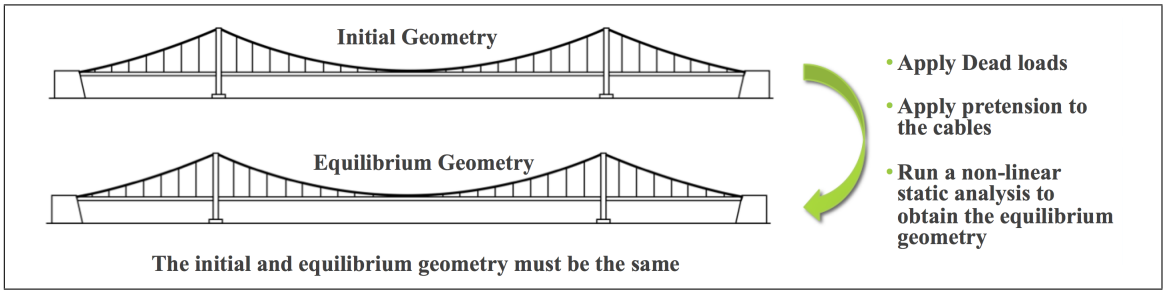

Figure 2.9. Procedure proposed by Ren et al. (2004)

Two exercises are presented in this document to validate cable modeling in ANSYS. The first one is a modal analysis of a single cable subjected to its self-weight, and the second is a 2D modal analysis of a simplification of the Great Belt Bridge.

2.5.1. Modal analysis of a single cable hanging under its own weight

The cable selected is shown in Figure2.10, and it was studied by Ali (1995) to present an isoparametric cable element and by Karoumi (1999) to verify his catenary cable element and compare it with the one proposed by Ali. The cable is hanging under its self-weight and is subjected to an horizontal tension T_0. The unstressed length of cable is $L_u = 312.7$ m, the modulus of elasticity is $E = 1.31 \cdot 10^{11}$ N/m^2, it has a cross section area of $A = 5.48 \cdot 10^{-4}$ m^2, and a weight per unit of length $w = 46.11$ N/m. The initial distance of the supports of the cable is 304.8 m and the initial sag of the cable is 30.48 m (sag to main span ratio of 1/10). The force T_0 in the cable to achieve the equilibrium position is $1.7794 \cdot 10^4$ N.

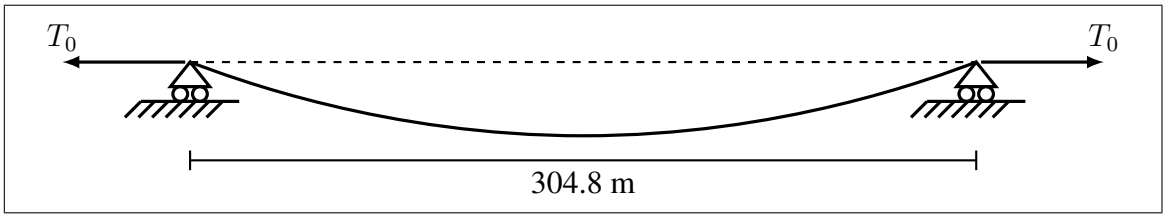

Figure 2.10. Cable used for modal analysis

The first step was to find the target configuration of the cable, in this case, the configuration described above. As the cable is only subjected to its self-weight, it was supposed as a catenary, thus the initial shape was determined with Equation 2.6. In a first attempt, the cable was modeled with 20 elements, 21 points and assuming the catenary geometry described before. The next step was to find the initial strain of the elements by the trial and error method, and then the maximum deformation of the cable from its target configuration was analyzed.

Figure 2.11 shows the conducted analysis to obtain the prestrain of the cable elements. It can be seen that, for a cable subjected to its self-weight, a large pretension implies large positive deflections (it becomes a taut string), which results in a smaller sag than the target one and a larger horizontal force. On the other side, small pretension implies almost 0 deflection and the wanted tension on the cable. In conclusion, in the case of a simple cable under its self-weight a small prestrain is enough to achieve the wanted configuration. However, ff the input prestrain is set as 0, there is not initial stiffness in the cables and the method does not find a solution.

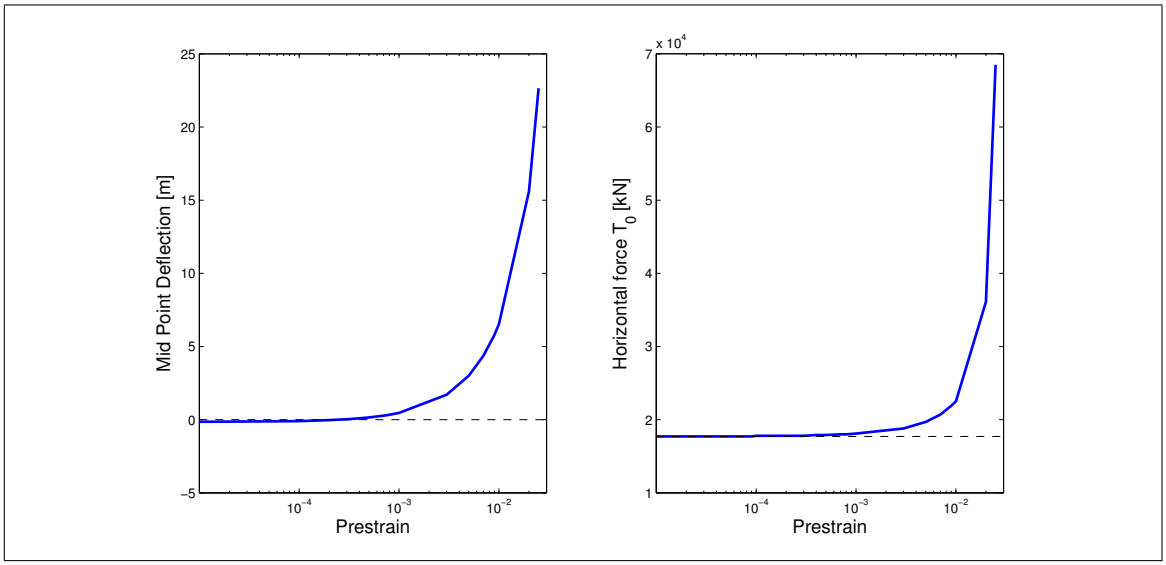

Figure 2.11. Influence of the initial prestrain on mid point deflection and T_0

Based on the previous analysis, an initial prestrain of $5 \cdot 10^{-4}$ [m/m] is chosen for conducting a modal analysis of the cable. The modal analysis of structures with cable elements must be done in two steps. The first step is to obtain the equilibrium condition of the structure when subjected to gravity loads. Then, the modal analysis is specified in ANSYS as a perturbed modal analysis, which uses the stiffness matrix of the last step of the previous static analysis to calculate the eigen-values. The Block-Lanczos method is selected to calculate the eigen-values of the system (Grimes, Lewis, & Simon, 1994). Figure 2.12 displays the shape of the first 4 vertical modes of the cable, and Table 2.1 shows a comparison between the vertical frequencies obtained on ANSYS and those calculated by the equations shown in Figure 2.5.

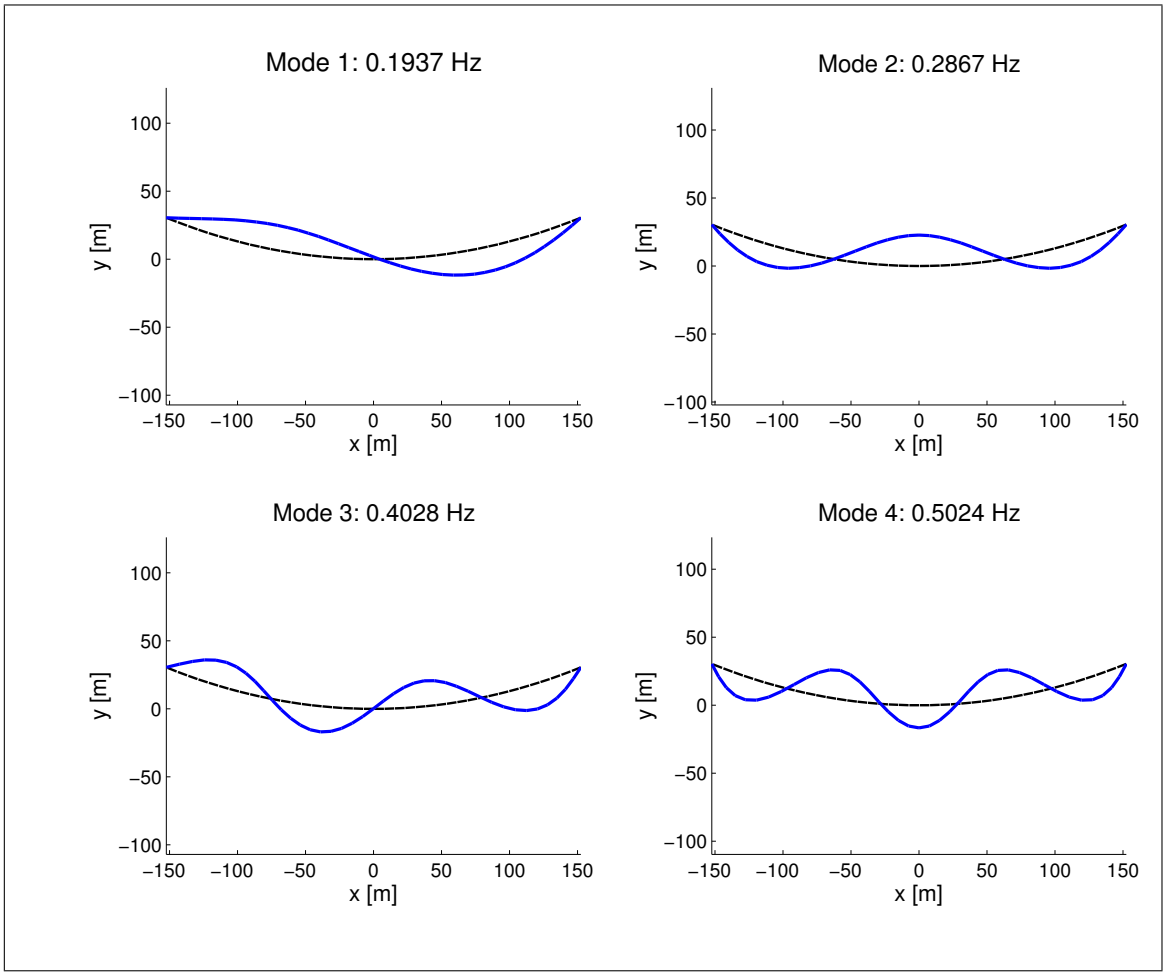

Figure 2.12. Modes and frequencies of the cable obtained with ANSYS

Table 2.1. Comparison between theoretical and ANSYS vertical frequencies

Mode	Theoretical [Hz]	ANSYS [Hz]	Error [%]
1	0.2019	0.1937	4.0443
2	0.2887	0.2867	0.7017
3	0.4037	0.4028	0.2298
4	0.4964	0.5024	-1.2121

The shapes of the modes obtained with ANSYS are very similar to those of Figure 2.5, and the frequencies obtained are really close to the theoretical ones. The differences can be explained by the number of elements used on the analysis and the elasticity of the cable, since the formula of Figure 2.5 assumes an inextensible cable.

The sway modes can also be obtained by allowing the cable to move in its transverse direction. Figure 2.13 shows the first two sway modes obtained with ANSYS. The theoretical values for the modal frequencies are 0.1010 Hz and 0.2020 Hz for the first and second sway modes respectively (calculated with Equation 2.10), which shows a very good agreement with the ones obtained with ANSYS (with 0.89% and 0.94% of error).

2.5.2. Great Belt Bridge

The Great Belt (Storebaelt) Suspension Bridge, built in Denmark and open to traffic in 1998, has the third largest span in the world with 1624 m main span (Table 1.1), and two side spans of 535 m. One of the main features of the bridge is that it has a continuous suspended deck as can be seen in Figure 2.14, i.e., it is not vertically supported by the pylons (Gimsing & Georgakis, 2012). The sag to main span ratio of the bridge is 1/9, and the main cables are anchored to the bridge at the sag point of the main span with central clamps.

Karoumi (1999) made a 2D model of the Great Belt Bridge in order to validate his catenary cable element using MATLAB. For that purpose, he made a frequency analysis and compared his results with the frequencies obtained from a 1:200 scale aeroelastic

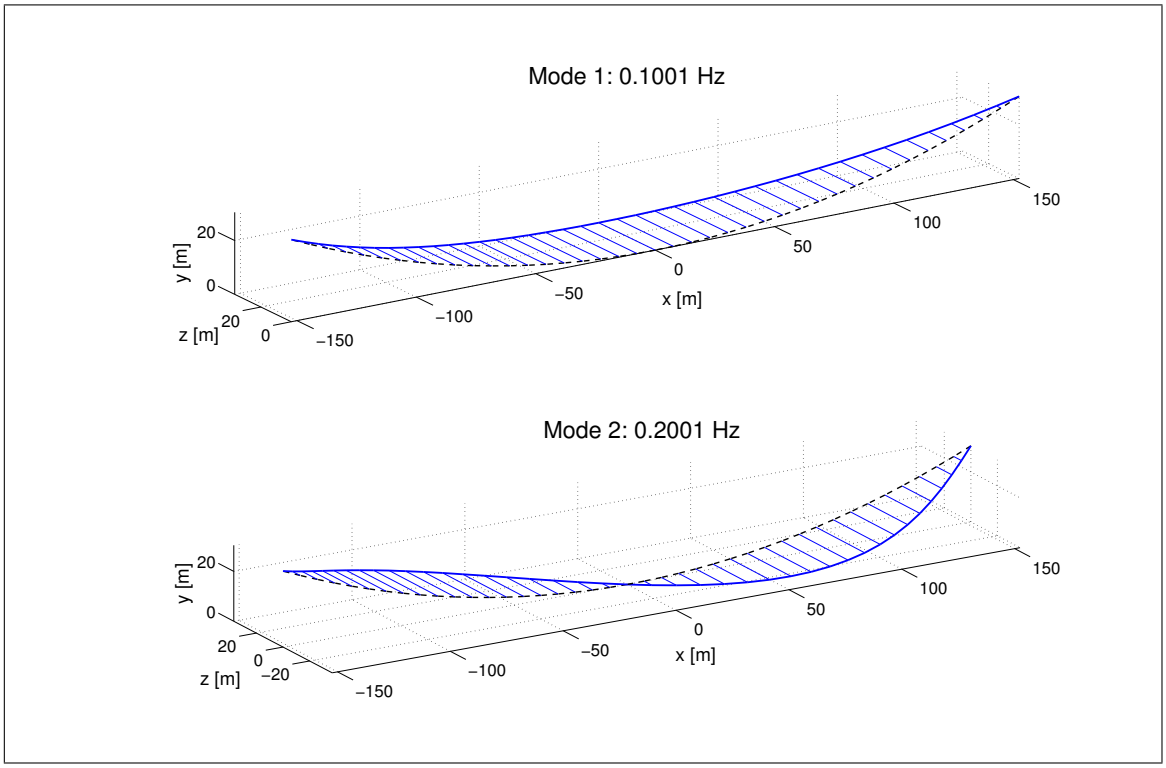

Figure 2.13. Sway modes obtained with ANSYS

Figure 2.14. Great Belt Bridge

bridge model made for wind tunnel testing (Larsen, 1993). For the numerical model, he considered every third hanger from the original bridge, and assumed that the self weight of the hangers and clamps were uniformly distributed along the main cable. The girder

was pinned at the ends, and the properties of the pylons were assumed by Karoumi to give the first and second pylon frequencies of 0.147 and 0.803 Hz respectively. The geometry of the bridge is shown in Figure 2.15, and the properties of the elements used by Karoumi in Table 2.2.

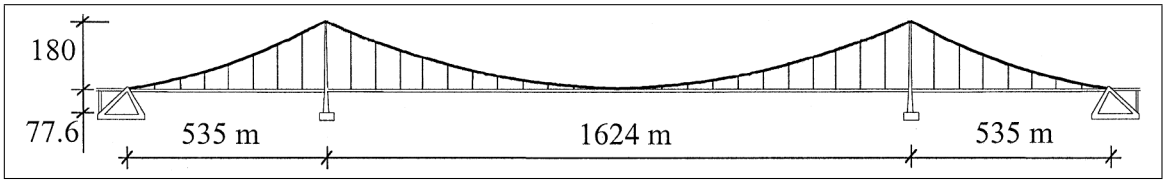

Figure 2.15. Geometry of the Great Belt Suspension Bridge (Karoumi 1999)

Table 2.2. Parameters for the model of the Great Belt Suspension Bridge (Karoumi 1999)

Member	E [GPa]	A [m^2]	I [m^4]	w [kN/m]
Girder	210	0.50	1.66	72.4
Pylon (0 - 75.5m)	40	37.5	750	882
Pylon (75.5 - 136.2 m)	40	32.5	275	764.4
Pylon (136.2 - 196.9 m)	40	30.0	200	705.6
Pylon (196.9 - 257.6 m)	40	25.0	150	588.0
Cable side spans	210	0.41	-	33.8
Cable main spans	210	0.40	-	32.9
Hangers	210	0.025	-	-

To validate the modeling of suspension bridges in this thesis, the Great Belt Bridge was modeled in ANSYS. The deck and pylons are modeled with BEAM188 elements, and the main cable and hangers with tension-only LINK180 elements. As the shape of the cable isn't described in Karoumi's article, Equation 2.4 is used, assuming that the cable is subjected to a constant vertical load from its self-weight and the dead load of the deck. The tension of the main cables was initially estimated with Equation 2.5, obtaining $H =$ 194,653 kN. Because it is a 2D model, displacement on the z axis, and rotations around the x and y axis were restrained.

The analysis was conducted using the same procedure as the one used in the cable of the previous section. Once again, the first step is to find the initial prestrain of the main cables by the trial and error method. Table 2.3 shows the maximum deflection of the bridge and the horizontal force T_0 of the main cablea for different values of prestrain.

It can be seen that with a low prestrain, the bridge has large deflections, which means that the deck is supporting a considerable part of the weight of the bridge. As the prestrain increases, the deflection decreases, and the force on the main cables increase because they start to take all the dead load of the girder. Finally, the tension of the main cables reaches a tension of $H = 192{,}965$ kN, with a difference of 0.8% with the tension estimated above (194,653 kN). A prestrain of 2x10^{-3} was chosen to conduc the modal analysis because it has very low deflections and the cable force is really close to the estimated with Equation 2.5. The frequencies and shapes of the vertical modes are displayed in Figure 2.16, and Table 2.4 shows a comparison between the frequencies obtained with ANSYS, by Karoumi (1999) and the wind tunnel. The obtained mode shapes (Figure 2.16) for the three first modes are really close to those obtained by Karoumi, and the frequencies also shows a very good agreement with both sources.

Table 2.3. Cable prestrain influence of the Great Belt Bridge. Negative values for deflections represent an upward movement. The row marked in black indicates the value of prestrain used in the model.

Prestrain	Cable Force T_0 [kN]	Deflection [m]
1x10^{-5}	177,620	9.5821
1x10^{-4}	179,452	9.2046
1x10^{-3}	186,556	5.3804
2x10^{-3}	192,956	1.1723
3x10^{-3}	199,820	-3.3820
5x10^{-3}	223,172	-12.4244

The first frequency obtained with ANSYS is just 3% lower than the one obtained by Karoumi, and 4% lower with the obtained on the wind tunnel experiment. The second

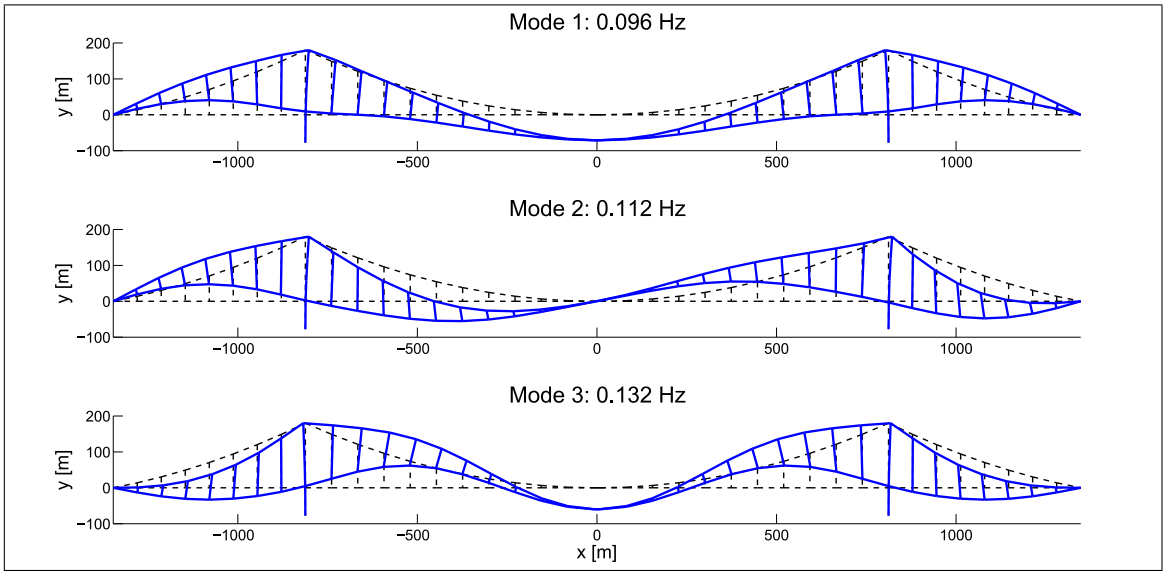

Figure 2.16. Vertical Great Belt Bridge Modes

Table 2.4. Vertical frequencies of the Great Belt suspension bridge

Mode	ANSYS [Hz]	Karoumi [Hz]	Wind Tunnel [Hz]
1	0.096	0.099	0.100
2	0.112	0.112	0.115
3	0.132	0.130	0.135

and third frequencies also show good agreement with the Karoumi's element and the wind tunnel. The presented numerical models shows that cable elements and suspension bridges can be modeled with ANSYS and the obtained results are confirmed by other researches or by empirical values. The method described in this chapter is used to model the chosen example of a Longitudinally Asymmetrical Multi-Span Bridge, the Chacao Bridge.

3. THE CHACAO BRIDGE

The Chacao Bridge, a multi-span suspension bridge, will be constructed in the Chacao Channel in Chile, approximately 1,000 km south of Santiago (Figure 3.1) . It will connect mainland Chile with Chiloé Island, providing conectivity with the Route 5, the Pan-American road of the country. Nowadays, the only way to travel to Chiloé is by thirty minutes ferry across the Chacao Channel or by plane.

The idea of the Chacao Bridge arose in the past century, but it was in 2001 when the first designs were presented. One of them was two consecutive suspension bridges (as the San Francisco - Oakland Bay Bridge) and the other was a continuous two main spans suspension bridge. Both designs were longitudinally asymmetrical because the foundation of the central pylon was place in the Remolino Rock, which is situated slightly closer to the Chiloé Island than the northern mainland shore (Forsberg, 2001). This latter project was

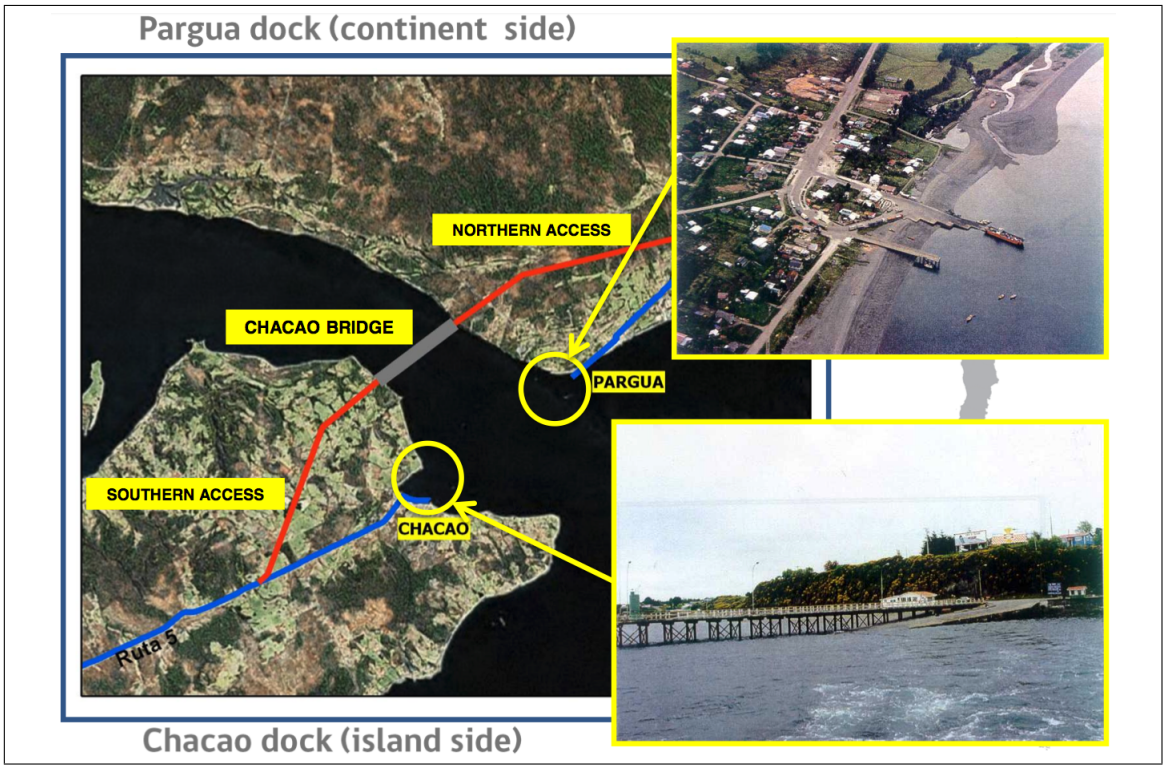

Figure 3.1. Location of the Chacao Bridge.

awarded by the Ministry of Public Works in 2005, but then it was rejected in 2007 due to economical constraints. In 2014 the bridge project was reactivated by the Ministry of Public Works and it was awarded to a new consortium (Valenzuela & Marquez, 2014b). By mid 2015, field works have already started and the bridge is in its final stage of design. The bridge is scheduled to be operating by 2020 and it will be the first longitudinal asymmetrical multi-span bridge in the world, which is reflected in the length of the two main spans and the heights of the three pylons.

The Chacao Bridge will be located in a highly seismic region due to the subduction of the Nazca plate under the South American plate, where the convergence plate rate is 66 mm/year (Angermann, Klotz, & Reigber, 1999). The bridge will be located near the rupture area of the Valdivia Earthquake (1960, Mw = 9.5), the largest recorded earthquake in the world. The Chacao Channel has average winds of 23.4 m/s, tidal variations of 5.74 m, and current flows of 5.28 m/s (Valenzuela & Marquez, 2014a).

The length of the current design of the Chacao Bridge (as of March 2015) is 2.75 km. It has two main spans: 1,055 m in the south span and 1,155 m in the north span, and it will be the bridge with the longest span in Latin America (Figure 3.2). The north side span has 284 m and at the south it considers an approach bridge of 140 m long with three spans of 43, 54 and 43 m. The suspension deck is a 25 m width orthotropic steel box girder, allowing it to have four traffic lanes (Figure 3.3). The thickness of the plates of the steel box is 8 mm, except the upper plate with 14 mm. The box girder also considers longitudinal stiffeners of 6 mm, and 8 mm thickness. The deck is continuous from the south pylon to the north abutment, and it is vertically supported in those points. The three pylons have lateral support devices to restrict the movement of the deck in the transverse direction.

The suspension bridge system is composed of two main cables that are restrained by two gravitational anchor blocks made of reinforced concrete that are located at the ends of the bridge. The sag-to-span ratio is 1/8.5 in the north span (calculated from the elevation at the north pylon) and 1/9.5 in the south span (calculated from the elevation at the central

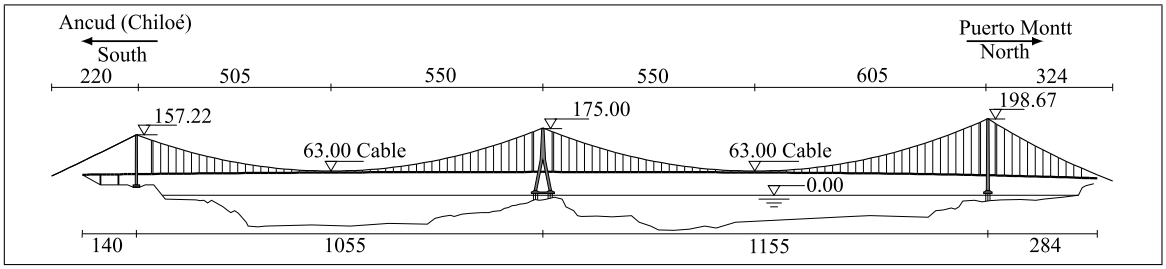

Figure 3.2. Elevation of the design of the Chacao Bridge (as of March 2015). The dimensions above the bridge indicate the main cables position, and the ones below the bridge indicate the length of the spans. Units in meters.

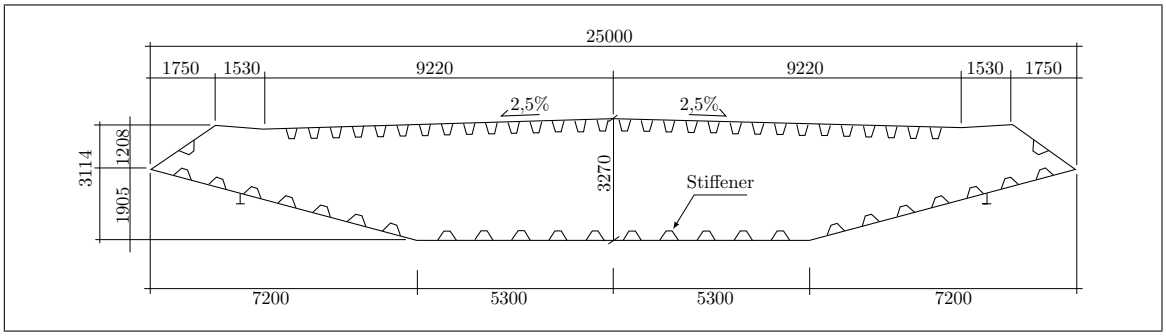

Figure 3.3. Cross section of steel box girder. All the dimensions are outer dimensions. Units in milimeters.

pylon), and the transverse distance between the main cables is 22.2 m. The main cables are formed by strands, which are precast steel wires with strength of 1860 MPa with hexagonal cross section. These strands are proposed to be installed with the Pre-fabricated Parallel Wire Strand (PPWS) technique. The hangers are arranged throughout the continuous deck and the typical distance is 20 m, except in the zones near the pylons and maximum sag. At the two points of maximum sag, central clamps are not considered and the minimum length of the hanger at this location is 3.18 m.

The bridge system is also comprised of three reinforced concrete pylons (Figure 3.4). The elevations of the south, central and north pylons, measured from the mean sea level to the top of the saddles are 157.22 m, 175.00 m, and 198.67 m respectively. The south and north pylon have an I shaped geometry, while the central pylon has an inverted Y

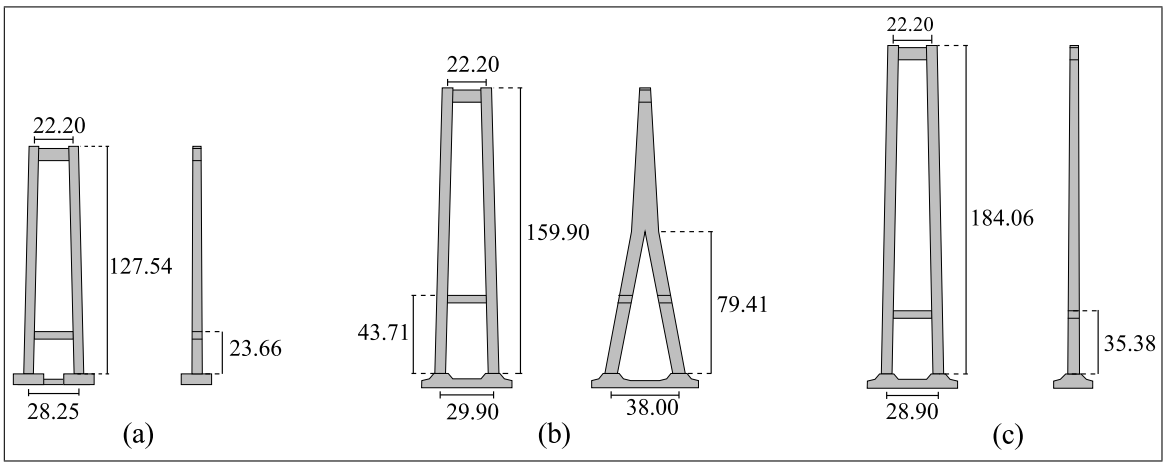

Figure 3.4. Dimensions of the pylons. (a) South pylon (b) Central pylon (c) North pylon. Units in meters.

shape. The shape of the central pylon is a major change from the project of 2001, where an A-shaped pylon was considered in order to control the top displacements of the tower. However, the A-shaped geometry induced high stresses in the legs and it provided a reduced safety factor for slipping of the cable in the saddles (Valenzuela & Marquez, 2014a). The three pylons are designed with upper and a lower cross beams, and the deck is supported vertically by the lower cross beam of the south pylon. The central and north pylon are founded under the sea and the south one on a plateau on the south shore (in the island of Chiloé).

4. FINITE ELEMENT MODEL

A three-dimensional finite element model of the current design of the Chacao Bridge is conducted to obtain the dynamic characteristics of a longitudinally asymmetrical multi-span suspension bridge. Non-linear geometry is considered in the finite element model and the software ANSYS (ANSYS, 2013) is used. The model, which looks like a fish spine model, is shown in Figure 4.1 and a zoom of the central pylon is displayed in Figure 4.2. The X axis is longitudinal to the deck of the bridge, the Z axis is transverse to the deck and the Y axis corresponds to the vertical axis (Figure 4.1).

4.1. Element types

The legs and cross beams of the pylons are modeled with two node beam elements (BEAM188). The main cables and hangers are simulated with tension only truss elements (LINK180), which allows the simulation of slack compression cables (Ren et al., 2004). Since only the properties of the deck affect the dynamic characteristics of the bridge rather than it structural details (Xu et al., 1997), the deck can be modeled with plate elements or beam elements. In this case, beams elements are selected (BEAM188), and rigid elements are used for the connection between the deck and the hangers. A spring element (COMBIN14) is chosen for the vertical and transverse connections of the deck with the pylons.

4.2. Material properties

Four types of materials are considered in the model and their properties are summarized in Table 4.1. The density of the deck steel material (13,114 kg/m^3) is larger than that of common steel because it accounts for the self weight of the asphalt layer and the lateral defenses. The resulting weight per unit length of the deck is 105.14 kN/m. The Young's modulus of the rigid material is assumed to be 100 times larger than that of regular steel.

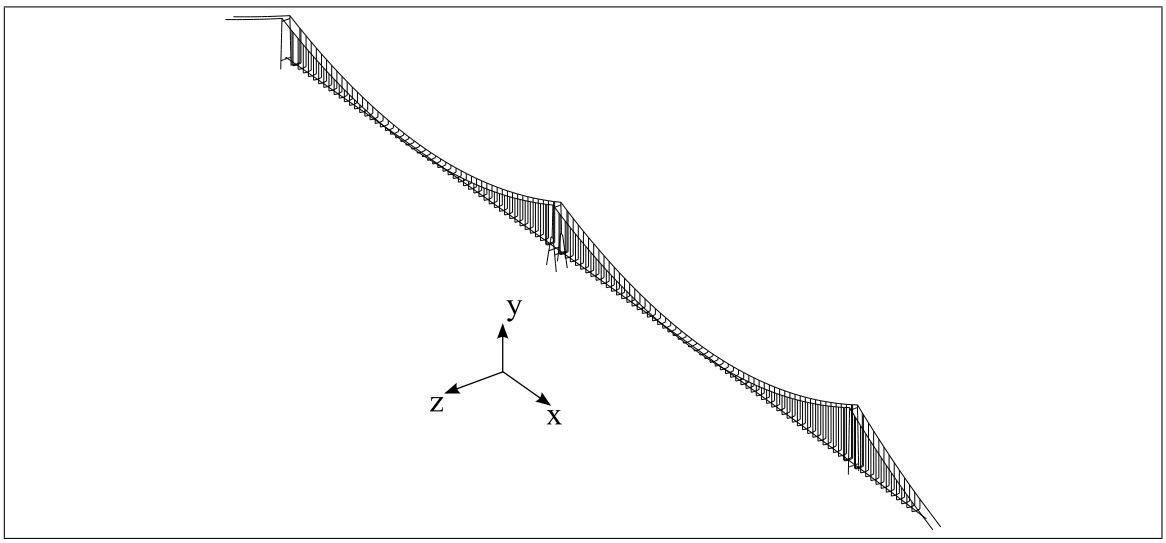

Figure 4.1. Finite element model of the Chacao Bridge with global axis

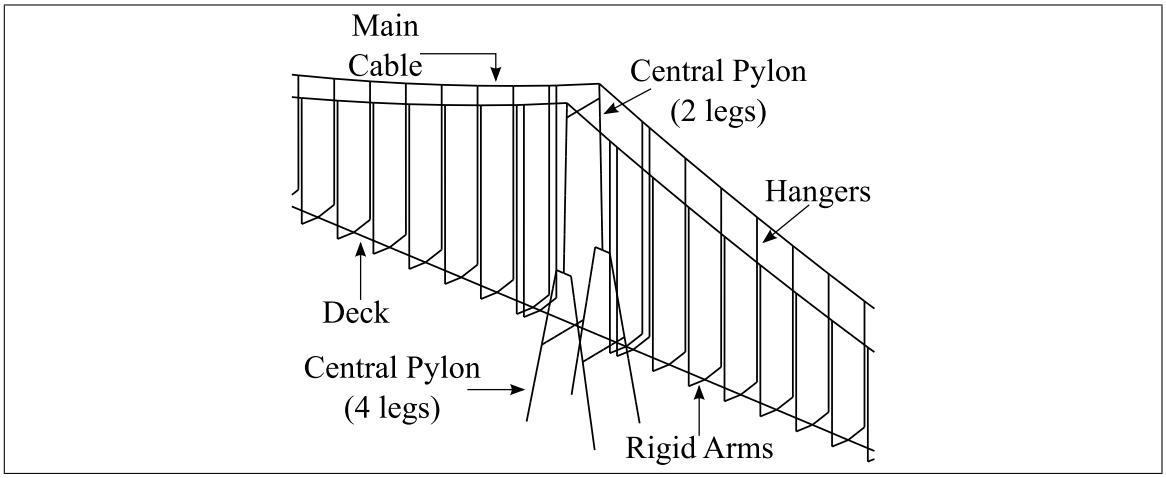

Figure 4.2. Zoom of the model with the elements

Table 4.1. Material properties.

Name	Elastic Modulus [GPa]	Poisson's Ratio	Density [kg/m^3]
Concrete	35.4	0.2	2,548
Cable steel	200.0	0.3	8,297
Deck steel	200.0	0.3	13,114
Rigid Material	2000.0	0.3	0

Table 4.2. Cross-section properties.

Pylon	Bottom width [m]	Top width [m]	Bottom depth [m]	Top depth [m]	Bottom thickness [m]	Top thickness [m]
South	5.788	5.122	5.464	5.466	1.1	0.5
North	6.657	5.352	6.000	6.000	1.1	0.5
Central (4 legs)	7.000	7.000	6.100	6.100	0.8	0.6
Central (2 legs)	15.667	6.100	6.100	6.100	1.2	0.5

4.3. Cross-section properties and weight of the bridge

The deck is modeled as a general section in ANSYS with the stiffness properties of the orthotropic steel box girder. The cross section area considered for this element is 0.855 m^2, the moment of inertia about the strong axis is 38.93 m^4, the moment of inertia about the weak axis is 1.29 m^4 and the torsional moment of inertia is 3.33 m^4.

The pylon legs and the cross beams are modeled as hollow rectangular cross sections with varying dimensions along the pylon height. Table 4.2 shows the maximum and minimum widths, depths, and thickness of the cross sections considered at the bottom and top of the legs of the pylons respectively. The row referred to "4 legs" of the central pylon in Table 4.2, corresponds to the elements from the bottom until the height of 79.41 m in Figure 3.4 (b), and "2 legs" of the central pylons corresponds to the elements above that height, as shown in Figure 4.2. The variation of these dimensions is linear over the height of the pylons.

The main cables of the bridge are modeled with a cross section area of 0.175 m^2, except in the north side span, where an area of 0.180 m^2 is used. An area of 0.0037 m^2 is considered for the typical hangers, except for the ones near the pylons that are modeled with an area of 0.0057 m^2. The total weight of the bridge in the model is 870,344 kN, in which the weight of the foundations and anchorage blocks are not considered as they are not part of the model.

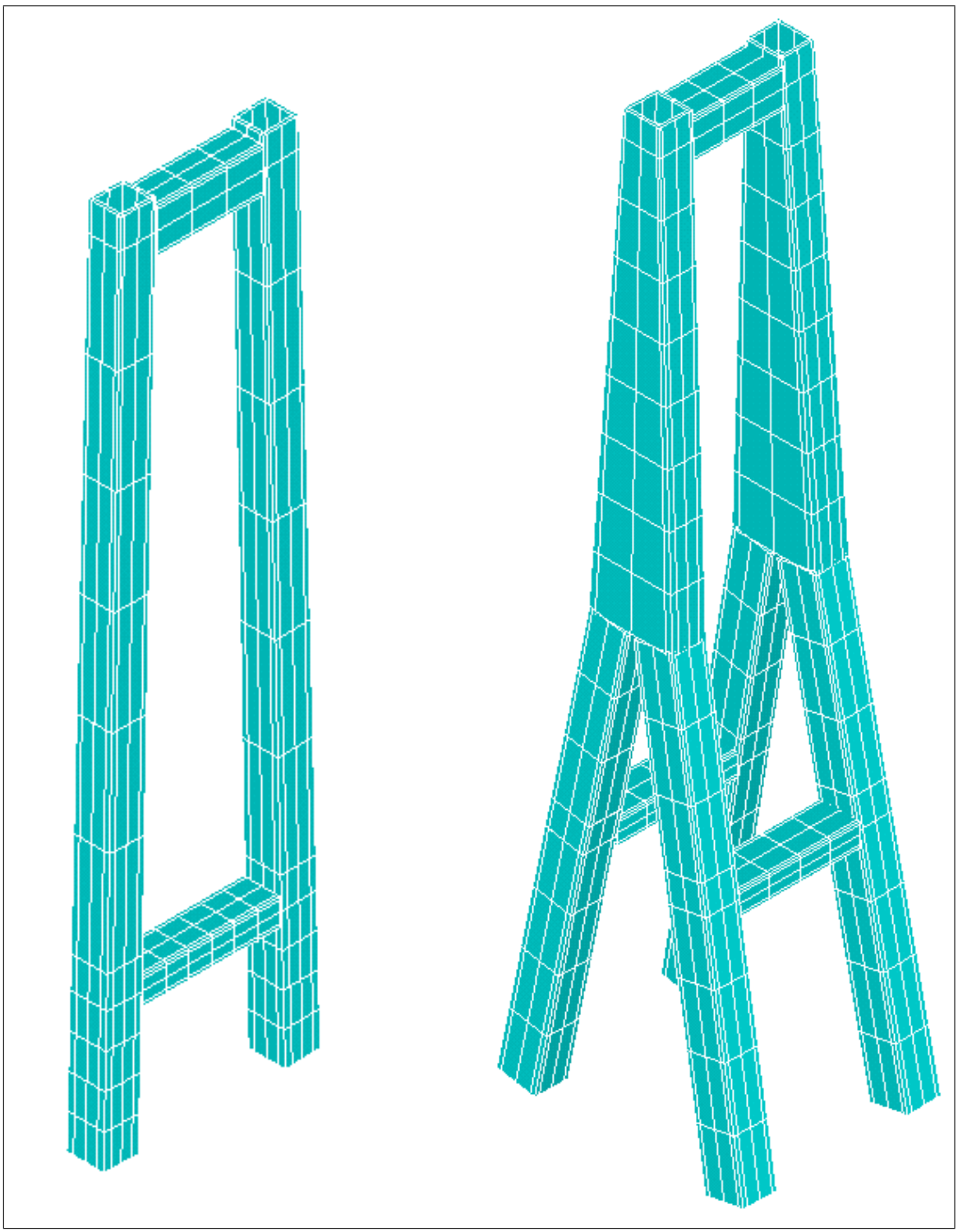

Figure 4.3. Isoparametric view of the model of the south pylon (left) and central pylon (right)

4.4. Boundary conditions

The legs of the three pylons are fixed at the base and the foundation stiffness is not incorporated in the proposed model. The deck is supported vertically in the south pylon using a link element (COMBIN14) with large stiffness and in the north abutment using a vertical support. The deck is restricted to move in the transverse direction in the three pylons and in the north abutment. The transverse constraint between the deck and the pylons is modeled with link elements from the deck to the pylons to transmit the transverse forces of the deck. In case of an extreme earthquake, the hydraulic buffers that support the deck in the longitudinal direction are intended to fail at a predefined maximum load avoiding excessive longitudinal forces being transferred through the deck. Therefore, in the proposed model, no restrains were considered in the bridge deck in the longitudinal direction. The main cables are fixed at the anchorage blocks and at the top of the pylons. Additionally, the three rotations of the cable nodes are restricted to remove these degrees of freedom.

4.5. Initial tension in main cables

The influence of the input prestrain of the main cables on the deck deflections is shown in Table 4.3. As prestrain increases, the deflection of the deck decreases, while the force in the main cable increases. When the prestrain exceeds the value of 2.7x10^{-3}, the deck experiments an upward deflection because the main cable starts carrying more vertical force than that required to maintain the initial geometry. From Table 4.3, it is concluded that negligible deflection at the two spans of the deck occurs for a prestrain of 2.7x10^{-3}, which is the chosen value for conducting the modal analysis in the next section.

Table 4.3. Main cables prestrain influence. Negative values for deflections represent an upward movement. The bold row indicates the value of prestrain finally used in the model.

Prestrain [cm/cm]	South span maximum deflection [m]	North span maximum deflection [m]	Cable Force [kN]
$1.0\text{x}10^{-5}$	6.694	7.423	84,726
$1.0\text{x}10^{-3}$	4.283	4.795	86,873
$2.0\text{x}10^{-3}$	1.808	2.104	89,192
$2.5\text{x}10^{-3}$	0.554	0.748	90,403
$2.7\text{x}10^{-3}$	**0.148**	**0.137**	**90,797**
$2.8\text{x}10^{-3}$	-0.208	0.162	91,115
$2.9\text{x}10^{-3}$	-0.461	0.361	91,903

5. MODAL ANALYSIS

The modal analysis of the bridge was carried out after the initial static equilibrium configuration was obtained. A perturbed modal analysis is conducted in ANSYS, which uses the tangent stiffness matrix of the equilibrium condition to calculate the eigen-values. The Block-Lanczos Method (Grimes et al., 1994) is selected to calculate the eigen-values and 500 modes were extracted.

The first ten vibration modes of the bridge are shown in Figure 5.1, where the transverse and vertical modes can be easily identified. The first transverse mode is the first mode of the bridge, its frequency is 0.0625 Hz, and it is characterized by asymmetric vibration of the main spans. The second transverse mode is the second mode of the bridge and its frequency is 0.0755 Hz. This second mode is characterized by symmetric transverse vibration of the main spans. The third and fourth transverse modes are the seventh and ninth modes of the bridge, and their frequencies are 0.1607 Hz and 0.1905 Hz, respectively. The third transverse mode is characterized by an asymmetric vibration with an entire wave on each span, and the fourth transverse mode is similar but both spans vibrate in a symmetric way.

The first vertical mode (f = 0.1115 Hz) is the third mode of the bridge. This mode is characterized by a large vertical vibration in the north span (an entire wave), the longest one, and a reduced vibration in the south span. The second vertical mode is the fourth mode of the bridge (f = 0.1205 Hz), and its mode shape is similar than that of the previous mode, but in the fourth mode the large vibration occur in the south span. The difference between the frequencies of these two modes is attributed to the difference between the lengths of the span with larger vibration. The next two vertical modes, the fifth and sixth modes of the bridge show a half wave vibration of each span with asymmetric and symmetric overall shape, respectively.

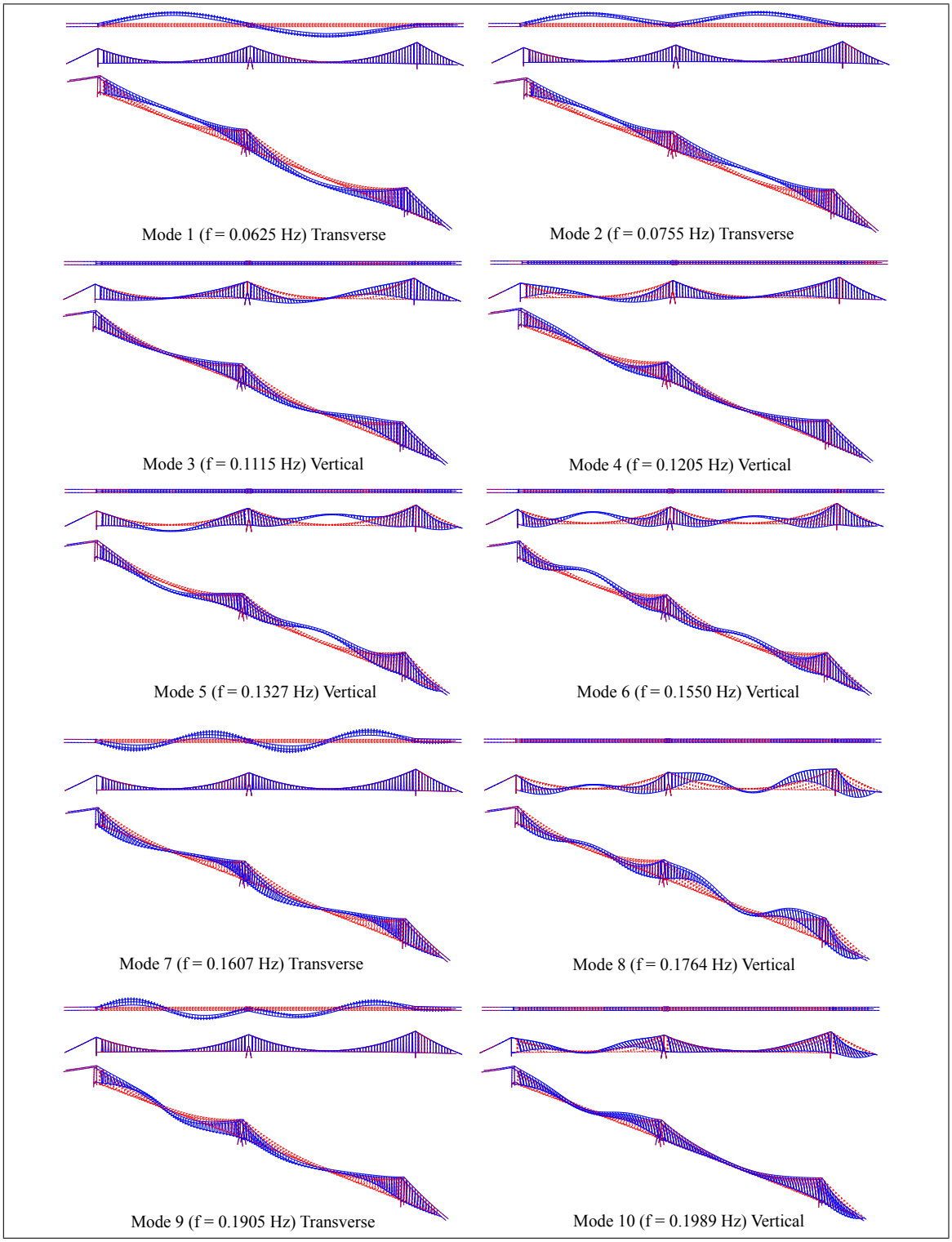

Figure 5.1. First ten vibration modes of the bridge (For each mode, a plan view, an elevation view and an isometric view is provided)

5.1. Comparison of the vibration modes with those from a similar bridge

The mode shapes and frequencies obtained with the model of the Chacao Bridge are compared with those of the Taizhou Bridge, a similar multi-span suspension bridge but with a longitudinal symmetric configuration (Wang et al., 2014). The comparison of the first ten modes is summarized in Table 5.1. The mode shape of the first mode of both bridges is equivalent, and it is characterized by asymmetric vibration of the main spans. However, the frequency of the first mode of the asymmetric bridge is 13% smaller than that of the symmetric bridge because the former has a longer span and a slender deck. The second mode of the asymmetric bridge is a transverse mode, unlike the second mode of the symmetric bridge which is a vertical mode. However, the second transverse modes of both bridges are similar, and are characterized by symmetric vibration of the main spans.

The largest difference between the first vibrations modes of the asymmetric and symmetric bridges occurs for the vertical modes. In the asymmetric bridge, the first two vertical modes, characterized by individual vibration of the main spans, are inexistent in the symmetric bridge. The third vertical mode of the asymmetric bridge is similar to the first vertical mode of the symmetric bridge and is characterized by vertical vibration of the two main spans. However, the frequency of this third vertical mode of the asymmetric bridge (f = 0.1327 Hz) is 66% larger than that of the vertical vibration mode of the symmetric bridge (f = 0.0802 Hz).

5.2. Modal contribution to base shear in the pylons

As the Chacao Bridge will be located in a highly seismic region in Chile, it is of interest to estimate the seismic base shear of the pylons. The question that wants to be answered here is which are the modes that have larger contribution to the response of the seismic base shear in the transverse and longitudinal direction of the three pylons. The identification of these modes is relevant for the design of a multi-span suspension bridge because they are required to conduct inelastic pushover analyses of the individual pylons.

Table 5.1. Comparison of vibration modes of the longitudinally asymmetric Chacao Bridge and the symmetric Taizhou Bridge. AS = Asymmetric; S = Symmetric; T = Transverse; V = Vertical

	Asymmetric Chacao Bridge		Symmetric Taizhou Bridge (Wang et al., 2014)	
Mode	Frequency [Hz]	Mode shape description	Frequency [Hz]	Mode shape description
1	0.0625	AS-T vibration of the deck	0.0716	AS-T vibration of the deck
2	0.0755	S-T vibration of the deck	0.0802	AS-V vibration of the deck
3	0.1115	V vibration of north span	0.0951	S-T vibration of the deck
4	0.1205	V vibration of south span	0.1149	A-V vibration of the deck
5	0.1327	AS-V vibration of the deck	0.1176	S-V vibration of the deck
6	0.1550	S-V vibration of the deck	0.1371	S-V vibration of the deck
7	0.1607	S-T vibration of the deck	0.1701	AS-V vibration of the deck
8	0.1764	AS-V vibration of the deck	0.1852	S-V vibration of the deck
9	0.1905	AS-T vibration of the deck	0.2306	AS-T vibration of the deck
10	0.1989	S-V vibration of south span	0.2379	AS-V vibration of the deck

In order to identify the modal contribution to the response, the modal static and modal dynamic responses are obtained following Chopra's approach (Chopra, 2012).

The modal static response to base shear V_{bn}^{st} is obtained by static analysis using the modal expansion $\mathbf{s}_n$ of the applied force distribution $\mathbf{s} = \mathbf{M}\boldsymbol{\iota}$, defined as:

$$\mathbf{s}_n = \Gamma_n \mathbf{M} \boldsymbol{\phi}_n \tag{5.1}$$

Where $\mathbf{M}$ is the mass matrix, $\boldsymbol{\iota}$ is the influence vector for the earthquake in the longitudinal or transverse direction, Γ_n is the modal participation factor and $\boldsymbol{\phi}_n$ is the mode shape of the n-th mode.

The modal static base shear V_{bn}^{st} of each pylon was obtained from the modal reactions obtained in ANSYS, which were multiplied by Γ_n/ω_n^2 as the applied modal forces in ANSYS are:

$$f_n = \mathbf{K}\phi_n = \mathbf{M}\phi_n\omega_n^2 = \frac{\mathbf{s}_n\,\omega_n^2}{\Gamma_n} \tag{5.2}$$

Table 5.2. Modal contribution factors to base shear (r_n) and modal base shear (V_{bn}) in both directions for the central pylon.

Central Pylon Transverse Direction					Central Pylon Longitudinal Direction				
Mode	Frequency [Hz]	$\overline{r}_n$	Sa [m/s^2]	V_{bn} [%W]	Mode	Frequency [Hz]	$\overline{r}_n$	Sa [m/s^2]	V_{bn} [%W]
2	0.075	0.309	0.098	0.138	5	0.133	0.040	0.174	0.030
19	0.290	0.019	0.463	0.039	6	0.155	0.015	0.212	0.014
29	0.367	0.053	0.622	0.149	10	0.199	0.389	0.289	0.498
30	0.368	0.027	0.624	0.076	11	0.209	-0.042	0.309	0.057
36	0.427	0.251	0.753	0.860	81	0.850	0.143	1.777	1.124
45	0.494	0.059	0.903	0.241	95	0.991	-0.016	2.152	0.153
143	1.530	0.020	3.704	0.340	128	1.343	0.030	3.149	0.412
145	1.551	0.030	3.770	0.517	149	1.574	0.016	3.840	0.271
150	1.580	0.020	3.856	0.349	151	1.607	0.321	3.942	5.598
157	1.661	0.027	4.106	0.509	186	2.006	0.034	5.200	0.778
	$\sum \overline{r}_n$	0.814	$\sqrt{\sum V_{bn}^2}$	1.269		$\sum \overline{r}_n$	0.929	$\sqrt{\sum V_{bn}^2}$	5.807

Where $\mathbf{K}$ is the tangent stiffness matrix of the static equilibrium condition and ω_n the angular frequency of the n-th mode.

The modal contribution factor to the base shear is obtained as:

$$\overline{r}_n = \frac{V_{bn}^{st}}{V^{st}} \tag{5.3}$$

Where V^{st} is the static value of the base shear in the corresponding pylon due to the external forces $\mathbf{s}$. Tables 5.2, 5.3 and 5.4 summarizes the values of $\overline{r}_n$ for the base shear of the three pylons (central, north and south) for the transverse and longitudinal direction. The ten modes with larger values of $\overline{r}_n$ are shown for each case, and the sum of this factors is displayed at the end of the respective column.

For the transverse direction, the largest static modal contribution to the base shear (largest $\overline{r}_n$) of the three pylons is given by the second mode, as the deck is pushing the three pylons in the same direction. The second mode with the largest contribution differs for the three pylons (mode 36, 14 and 41 for the central, north and south pylon, respectively).

Table 5.3. Modal contribution factors to base shear (r_n) and modal base shear (V_{bn}) in both directions for the north pylon.

North Pylon Transverse Direction					North Pylon Longitudinal Direction				
Mode	Frequency [Hz]	$\overline{r}_n$	Sa [m/s^2]	V_{bn} [%W]	Mode	Frequency [Hz]	$\overline{r}_n$	Sa [m/s^2]	V_{bn} [%W]
2	0.075	0.322	0.098	0.097	3	0.111	0.051	0.140	0.016
14	0.247	0.190	0.379	0.221	10	0.199	0.399	0.289	0.257
19	0.290	0.170	0.463	0.241	11	0.209	0.088	0.309	0.061
21	0.298	0.014	0.479	0.020	50	0.540	0.020	1.008	0.045
39	0.449	0.015	0.802	0.037	52	0.543	0.104	1.014	0.235
65	0.671	0.028	1.322	0.114	53	0.546	0.240	1.021	0.546
85	0.875	0.025	1.842	0.141	81	0.850	-0.075	1.777	0.299
113	1.181	0.028	2.680	0.227	128	1.343	0.044	3.149	0.309
122	1.266	0.056	2.923	0.501	151	1.607	-0.021	3.942	0.183
225	2.460	0.014	6.708	0.291	186	2.006	0.062	5.200	0.720
	$\sum \overline{r}_n$	0.861	$\sqrt{\sum V_{bn}^2}$	0.734		$\sum \overline{r}_n$	0.912	$\sqrt{\sum V_{bn}^2}$	1.162

Table 5.4. Modal contribution factors to base shear (r_n) and modal base shear (V_{bn}) in both directions for the south pylon.

South Pylon Transverse Direction					South Pylon Longitudinal Direction				
Mode	Frequency [Hz]	$\overline{r}_n$	Sa [m/s^2]	V_{bn} [%W]	Mode	Frequency [Hz]	$\overline{r}_n$	Sa [m/s^2]	V_{bn} [%W]
2	0.075	0.325	0.098	0.057	10	0.199	-0.073	0.289	0.013
29	0.367	0.053	0.833	0.300	81	0.850	0.514	1.777	0.563
30	0.368	0.030	1.120	0.164	95	0.991	0.200	2.152	0.265
36	0.427	-0.035	0.903	0.116	128	1.343	-0.055	3.149	0.106
41	0.464	0.202	0.622	0.059	151	1.607	0.161	3.942	0.390
45	0.494	0.072	5.944	0.532	186	2.006	-0.115	5.200	0.369
57	0.588	0.082	9.810	0.615	242	2.668	0.052	7.426	0.237
202	2.208	0.030	0.753	0.047	338	3.760	0.028	9.810	0.171
206	2.233	0.050	5.863	0.312	342	3.807	0.034	9.810	0.203
416	4.656	0.035	0.624	0.033	372	4.154	0.033	9.810	0.200
	$\sum \overline{r}_n$	0.844	$\sqrt{\sum V_{bn}^2}$	0.948		$\sum \overline{r}_n$	0.778	$\sqrt{\sum V_{bn}^2}$	0.924

These modes are characterized by transverse displacement of the individual pylons. For the three pylons, table 5.2 shows that the ten modes with larger static contribution represent up to 86% of the static response of the base shear in the transverse direction. If 40 modes are incorporated, this static contribution to the base shear increases to 95%.

For the longitudinal direction, the largest static modal contribution to the base shear of the central and north pylon is provided by mode 10, which induces longitudinal displacements at the top of the referred pylons. For the south pylon, the largest static contribution is given by mode 81. This mode also has a significant static contribution for the base shear of the central pylon ($\overline{r}_n$ = 0.143), and a smaller contribution for the base shear of the north pylon ($\overline{r}_n$ = -0.075). For the central pylon, the second mode with largest contribution to the base shear in the longitudinal direction is mode 151 ($\overline{r}_n$ = 0.321). This mode shape is characterized by coupled movement of the three pylons, which induces high longitudinal reactions in the base of these three towers. For the central and north pylon, Tables 5.2 and 5.3 show that the ten modes with larger static contribution accounts for about 92% of the static response of the base shear in the longitudinal direction. If five more modes are added, this static contribution increases to 95%. However, only 78% of the static contribution is obtained for the south pylon when ten modes are considered. For this pylon, near 26 modes would be required to reach a static contribution of 95%.

Tables 5.2, 5.3 and 5.4 also show the pseudo-acceleration (S_a) of each mode. The pseudo-acceleration spectrum considered here was elaborated specifically for the Chacao Bridge project in 2001 (MOP, 2001) considering a subduction earthquake with a probability of exceedance of 10% in 100 years. The spectrum considers 2% damping and is given by (in units of g):

$$S_a(T) = \begin{cases} 0.3 + \dfrac{28}{3}T & 0 \leq T < 0.075 \text{ [s]} \\ 1 & 0.075 \leq T < 0.3 \text{ [s]} \\ \dfrac{0.222}{T^{5/4}} & 0.3 \leq T < 11.94 \text{ [s]} \\ 0.01 & 11.94 \leq T \leq 20 \text{ [s]} \end{cases} \tag{5.4}$$

Finally, the last column of each pylon in Table 5.2, 5.3 and 5.4 display the modal base shear of each mode, which is calculated as:

$$V_{bn} = V_{bn}^{st}\, \overline{r}_n\, S_a \tag{5.5}$$

and is expressed as a percentage of the self-weight of the whole bridge (W = 870,344 kN).

The spectral ordinates for the base shear in the transverse and longitudinal direction of the central pylon are shown graphically in Figure 5.2. For the base shear in the transverse direction, the mode with the largest static contribution (mode 2) has a low frequency (0.075 Hz) and hence its contribution to the base shear is low. The mode with the largest contribution to the base shear in the transverse direction is mode 36 (V_{bn} = 0.860%W), which frequency is 0.427 Hz. In general, the 10 modes with larger $\overline{r}_n$ contributes significantly to the base shear in the transverse direction. However, additional modes with smaller $\overline{r}_n$ also contributes significantly to the base shear and they should be considered in estimating the total base shear. For example, the modal base shear of mode 298 (f = 3.327 Hz, $\overline{r}_n$= 0.014) is 0.268%W, and is largest than the modal contribution of some modes with the largest $\overline{r}_n$ (Table 5.2). For the longitudinal direction of the central pylon, the mode with the second largest static contribution, mode 151 ($\overline{r}_n$ = 0.321%W), also has a significant spectral ordinate (Figure 5.2 (b)). Therefore, most of the base shear in the longitudinal direction is provided by this mode (Table 5.2).

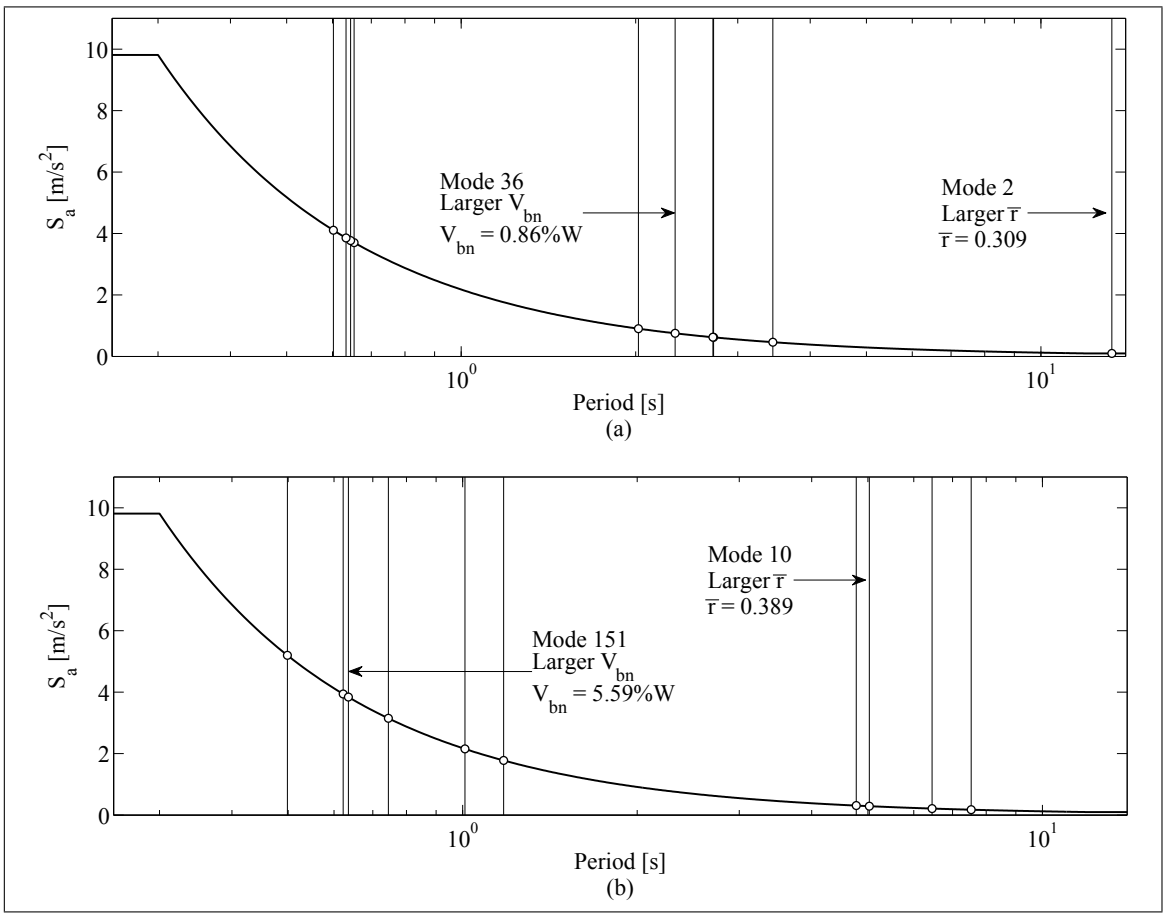

Figure 5.2. Natural periods and spectral ordinates for the base shear in the (a) transverse and (b) longitudinal direction of the central pylon of the bridge

Table 5.5 compares the base shear of the pylons calculated using 500, 10 and 1 mode, where SRSS method is used to combine the modal responses for simplicity. It is considered that 500 modes are adequate to estimate the base shear appropriately. For the case of 10 modes, the modes with largest static contribution are considered in each case (Tables 5.2, 5.3 and 5.4). For the case of 1 mode, the base shear is estimated with the mode with the largest contribution to the base shear for each case (largest V_{bn} in Tables 5.2, 5.3 and 5.4). The only good estimation obtained with one mode is the base shear of the central pylon in the longitudinal direction, with an error of 3.7%. Therefore, it is clear that mode 151 is the one that must be used for conducting a pushover analysis of this pylon in the longitudinal

Table 5.5. Base shear when considering 500, 10 and 1 modes. The error is calculated by comparing the base shear with that of 500 modes

Pylon	Direction	V_b [%W] 500 modes	V_b [%W] 10 Modes	Error %	V_b [%W] 1 Mode	Error %
Central	Transverse	1.504	1.269	15.6	0.860	42.8
	Longitudinal	5.815	5.807	0.1	5.598	3.7
North	Transverse	0.890	0.734	17.5	0.501	43.7
	Longitudinal	1.189	1.162	2.3	0.720	39.4
South	Transverse	1.05	0.948	9.7	0.615	41.4
	Longitudinal	0.945	0.924	2.2	0.563	40.4

direction. For the north and south pylons, the error in estimating the base shear in the longitudinal direction decreases when 10 modes are considered, and the largest error of 2.3% is obtained for the north pylon. For the base shear in the transverse direction, 10 modes are not enough as the error is larger than 0.7%, and more modes should be considered to estimate the base shear of the three pylons.

5.2.1. Longitudinal displacement at the top of the central pylon

The longitudinal displacement of the top at the central pylon is critical in multi-span suspension bridges because it produces deflections on the cables which may induce large vertical deflections on the deck. A longitudinal displacement of 7.61 cm is obtained considering 500 modes. This value seems to be small, but the order of magnitude can be verified with simple calculations. The fundamental frequency of the central pylon itself along the longitudinal direction is 0.9525 Hz. The modal coordinate corresponding to the top displacement is $\phi_{top} = 5.8\text{x}10^{-4}$, the modal participation factor is $\Gamma = 2863.7$, and the corresponding spectral displacement is $S_d = S_a/\omega^2 = 0.0572$ m. Therefore, the longitudinal displacement at the pylon can be estimated considering only this mode as:

$$\delta_{top} = \phi_{top} \cdot \Gamma \cdot S_d = 9.5 \text{ cm} \tag{5.6}$$

From the presented analysis, it is concluded that the seismic longitudinal displacement at the top of the central pylon is small. However, the central pylon may have larger displacements under traffic load over one of the main spans, which is the critical traffic load for multi-span suspension bridges.

6. PARAMETRIC ANALYSIS

As mentioned before, the central pylon is a critical element of multi-span suspension bridges. Three typical types of pylons are common in suspension bridges: I-shape, A-shape and inverted Y-shape. The main differences between them is their longitudinal stiffness, the stress in their legs and the safety factor of sliding resistance of the main cables. In the case of the Chacao Bridge, an inverted Y-shape was selected for the central pylon.

6.1. Central clamp

When a classic suspension bridge (one main span and two side spans) has an asymmetric traffic load in half of its main span, the main cables deflect in the longitudinal direction at midspan, which induces vertical deflections of the main deck (upward in the span without traffic load and downward in the span with traffic load) (Gimsing & Georgakis, 2012). The longitudinal displacement of the main cables and the vertical displacement of the deck can be reduced by anchoring the main cables to the deck with central clamps at the point of maximum sag. These clamps also helps to reduce the buffeting and flutter stability of the bridge (Wang, Zou, Li, & Jiao, 2010). The Lillibaelt Bridge (1970) and the Great Belt Bridge (1998), in Denmark, were both designed with central clamps to control longitudinal vibration and displacements. However, the Akashi Kaikyo Bridge, the Tsing-Ma Bridge and the Taizhou Bridge were designed without central clamps. The effect of central clamps in multi-span suspension bridges have been studied by Wang et al. (2014), who did a parametric analysis to study their influence in the dynamic properties of the bridge. Wang concluded that central clamps improve the flutter stability of the bridge, but no studies were found that report the effect of central clamps on the seismic behavior of multi-span suspension bridges.

To assess the effect of using central clamps on the Chacao Bridge, four cases are analyzed, (i) without central clamps, (ii) with central clamps on the north span, (iii) with

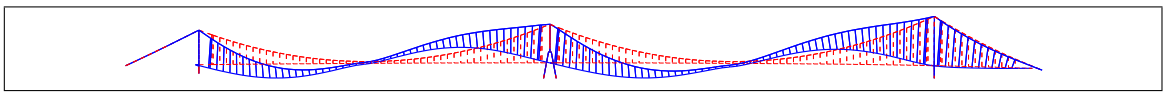

Figure 6.1. First vertical mode of the bridge with central clamps on both spans

central clamps on the south span, and (iv) with central clamps on both spans. The central clamps were incorporated in the described model by adding rigid elements between the main cables and the deck at the point of maximum sag. The modal frequencies of the first ten modes of the four cases are compared in Table 6.1. In the three cases where central clamps are included, the first and second frequencies increase slightly when comparing them with those of the original model. The most relevant effect are the changes of the frequencies and mode shapes related to vertical displacements of the deck (mode 3 and 4 of the original model). When central clamps are provided on the north span, the third mode corresponds to vertical vibration of the south span (f = 0.1174 Hz) and not on the north span (like mode 4 of Figure 5.1). The fourth mode for this case (f = 0.1304 Hz) is characterized by asymmetric vibration of both spans, with less displacements in the south span. On the other side, when central clamps are considered on the south span, the third mode (f = 0.1121 Hz) is similar than that of the original model, which is characterized by vibration of the north span. The mode corresponding to vibration of the south span increase its frequency from 0.1205 Hz to 0.1356 Hz when central clamps are added on the south span. When clamps are provided on both spans, the third mode is characterized by vibration of both spans (f = 0.1196 Hz, Figure 6.1) and the mode shapes of the 3rd and 4th mode of the original model disappear. It is important to clarify that when central clamps are considered, the vertical mode shapes are affected by the longitudinal restrain of the deck. If the deck is considered fixed in the longitudinal direction, the first vertical modes and frequencies of the models with central clamps slightly changes.

The modal contribution factors and the modal contribution to the base shear in the transverse and longitudinal direction of the central pylon are analyzed in Figure 6.2. For each of the four configurations, the ten modes with larger $\overline{r}$ are shown. In Figure 6.2 (a), the changes in the modal contribution factors for the base shear in the transverse direction

Table 6.1. Comparison of vibration frequencies [Hz] of the bridge with different central clamps configurations

Mode	Original model (without clamps)	Central clamps on north span	Central clamps on south span	Central clamps on both spans
1	0.0625	0.0628	0.0629	0.0629
2	0.0755	0.0762	0.0761	0.0761
3	0.1115	0.1174	0.1121	0.1196
4	0.1205	0.1304	0.1327	0.1329
5	0.1327	0.1349	0.1356	0.1548
6	0.1550	0.1552	0.1551	0.1669
7	0.1607	0.1757	0.1699	0.1757
8	0.1764	0.1770	0.1768	0.1890
9	0.1905	0.2045	0.2063	0.2056
10	0.1989	0.2273	0.2251	0.2197

can be observed. The modal contribution factor of mode 2 is the largest one for the four cases. For the models with clamps, the numbers of the modes with largest contribution factors are different, and mode 36 of the original model is identified in the models with clamps by observing the mode shape. When the modal contribution to the base shear is analyzed (Equation 5.5), it is clear that the contribution of mode 2 decreases considerably and the contribution of mode 36 is relevant for all cases. However, Figure 6.2 (b) shows a significant contribution of high frequency modes for the cases with clamps (i.e. a modal base shear of 1.24%W is obtained for one mode of the bridge with central clamps on the north span).

For the base shear in the longitudinal direction, mode 151 of the original bridge maintain the largest contribution when central clamps are added. However, the modal contribution to the base shear for the original bridge ($\overline{r}_n = 0.32$) and the bridge with clamps in the north span ($\overline{r}_n = 0.32$) are 66% larger than those of the other two cases. For the base shear in the longitudinal direction, mode 151 by itself contributes more than 90% to the total base shear in the four cases.

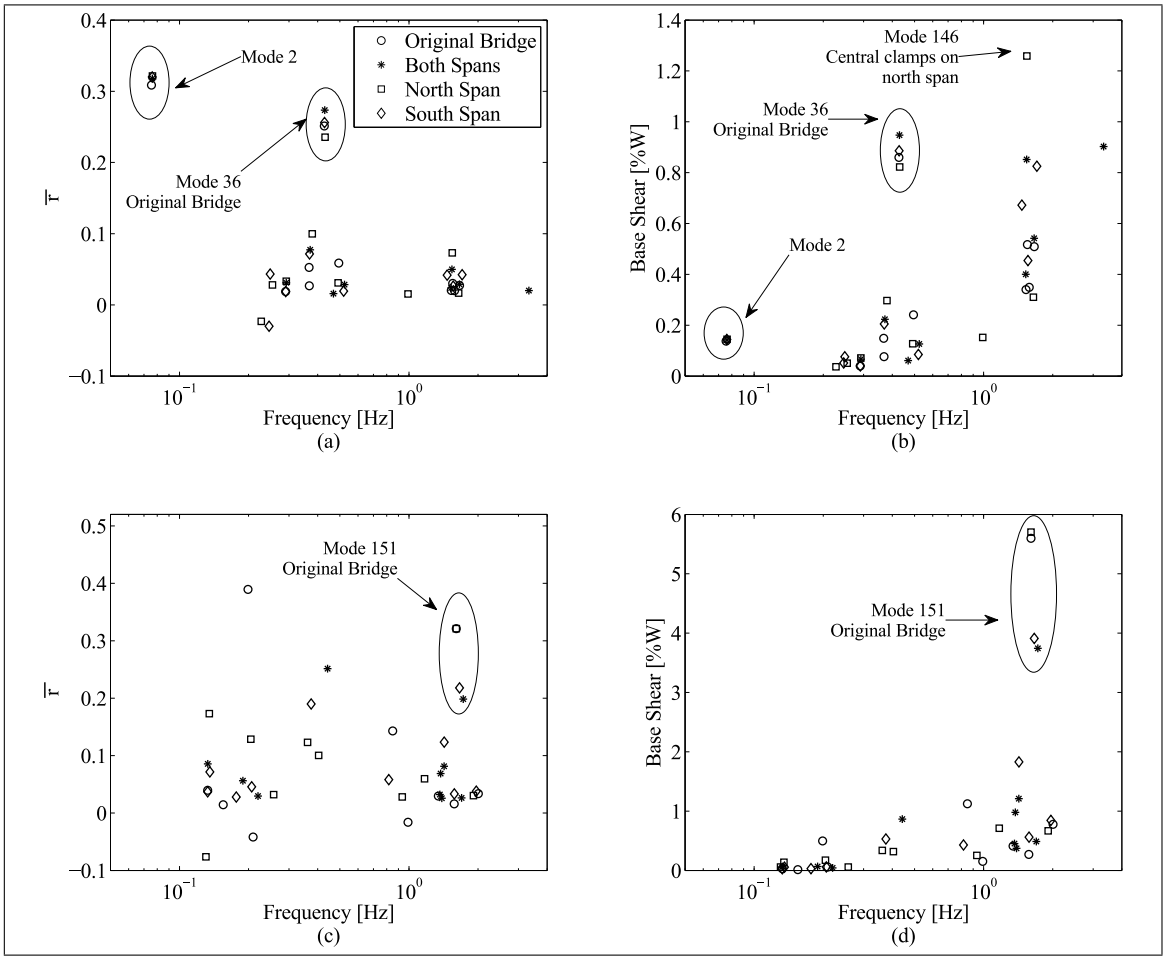

Figure 6.2. Modal contribution factors and modal contribution to base shear of the ten predominant modes for 4 cases: (i) original bridge, (ii) central clamps on north span, (iii) central clamps on south span and (iv) central clamp on both spans. (a) Modal contribution factors in the transverse direction, (b) Modal contribution to base shear in the transverse direction, (c) modal contribution factors in the longitudinal direction and (d), modal contribution to base shear in the longitudinal direction

Table 6.2 compares the total base shear of the three pylons and the longitudinal displacement at the top of the central pylon. For the four configurations of central clamps, the response was obtained using 500 modes in each case using SRSS modal combination. The base shear of the central pylon in the transverse direction increases when central clamps are considered. This increase is larger when central clamps are considered on both spans (19% increase) and the north span (19% increase), reflecting the influence of the mode 146

Table 6.2. Base shear for the three pylons and longitudinal displacement at the top of the central pylon with different central clamps configurations

Pylon	Direction	Base Shear [%W]			
		Original bridge	Central clamps on north span	Central clamps on south span	Central clamps on both spans
Central	Transverse	1.504	1.785	1.706	1.792
	Longitudinal	5.815	5.823	4.506	4.235
North	Transverse	0.890	0.638	0.782	0.890
	Longitudinal	1.189	0.801	1.546	1.086
South	Transverse	1.050	0.962	1.162	0.973
	Longitudinal	0.945	1.200	0.675	0.817
Longitudinal displacement of the top of the central pylon [cm]		7.61	4.82	5.54	7.62

(Figure 6.2 (b)). The base shear of the central pylon in the longitudinal direction decreases 22% and 27% when central clamps are considered in the south and north span respectively. It is concluded that central clamps are effective on controlling the longitudinal base shear of the central pylon as long as central clamps are considered in the south span. However, central clamps increase the base shear of the central pylon in the transverse direction.

The base shear in the transverse direction of the north pylon, the one with the side span, decreases 12% when central clamps are considered on the south span. For the longitudinal direction, the base shear decreases 33% and 9% when central clamps are considered on the north span and on both spans, respectively, and increases 30% when central clamps are considered on the south span. On the other side, the base shear in the two directions of the south pylon decreases when central clamps are considered on both span. If in the design stage of an asymmetric multi-span suspension bridge central clamps are an option, the four distribution cases must be evaluated, and their effect must be analyzed carefully depending on which pylon performance wants to be improved. If the base shear of the central pylon in the longitudinal direction is the critical value, it is recommended to provide central clamps on both spans of the bridge, but if the base shear in the transverse direction is critical, the

inclusion of central clamps is not convenient. Furthermore, despite the four cases improve the seismic behavior of some pylons in a particular direction, they might have a negative effect in other pylons. For example, the base shear in the longitudinal direction of the north pylon decreases 32% by adding central clamps on the north span, but that increases 27% the base shear in the longitudinal direction of the south pylon.

Finally, Table 6.2 shows that minimum seismic displacement at the central pylon is obtained when central clamps are provided in the north span (4.82 cm) and the largest displacement are obtained for the original bridge (7.61 cm) and the one with central clamps in both spans (7.62 cm). Therefore, the minimum displacements are not obtained for the case with central clamps on both spans. Central clamps are effective to restrain the displacements at the top of the pylons when the deck is fixed in one end (Gimsing & Georgakis, 2012), which is not the case of this model.

6.2. Stiffness of central pylon

As mentioned, the central pylon is a critical element of multi-span suspension bridges. Three typical types of pylons are common in suspension bridges: I-shape, A-shape and inverted Y-shape. The main differences between them is their longitudinal stiffness, the tension in their legs and the slipping resistance of the main cables. In the case of the Chacao Bridge, an inverted Y-shape was selected for the central pylon.

In this section, the influence of the stiffness of the central pylon on the dynamic characteristics of the bridge is analyzed. To vary the stiffness, the elastic modulus of the material of the central pylon ($E_c = 35.4$ GPa) is varied without changing the geometry of the central pylon, which would lead to a new design of the bridge. In this parametric study, the modulus of elasticity E_c is amplified by factors of 0.75, 1.00, 1.25 and 1.50. These values may represent realistic range of stiffness variations as larger variations may imply changes in the pylon geometry (i.e. A-shape pylon). Table 6.3 compares the modal frequencies of the bridge for the selected values of elastic modulus.

Table 6.3. Vibration frequencies [Hz] of the bridge for varying elastic modulus of the central pylon

Mode	$0.75E_c$	$1.00E_c$	$1.25E_c$	$1.50E_c$
1	0.0625	0.0625	0.0625	0.0625
2	0.0754	0.0755	0.0755	0.0755
3	0.1115	0.1115	0.1115	0.1115
4	0.1205	0.1205	0.1205	0.1205
5	0.1274	0.1327	0.1359	0.1379
6	0.1543	0.1550	0.1556	0.1560
7	0.1607	0.1607	0.1607	0.1607
8	0.1748	0.1764	0.1776	0.1785
9	0.1901	0.1905	0.1906	0.1908
10	0.1976	0.1989	0.1999	0.2006

The first two modes, that correspond to transverse vibrations of the deck and cables, are not affected by the stiffness of the central pylon, which agree with the results obtained by Ge & Xiang (Ge & Xiang, 2011). The mode 7, which is related to transverse vibration of the deck, is also not affected by the stiffness of the central pylon, and the frequency of mode 9 slightly increases as the pylon stiffness increases. It is concluded that the central pylon stiffness does not influence the dynamic characteristics of the low-frequency transverse modes. Regarding the vertical modes, the frequency of the first two vertical modes (modes 3 and 4) are not affected by the stiffness of the central pylon, but the frequencies of the next two vertical modes (mode 4 and 5) increases as the stiffness increases. This results are different than those obtained by Ge & Xiang, where the first vertical frequency increased with the increase of stiffness. However, Ge & Xiang analyzed a symmetric multi-span suspension bridge, which first vertical frequency corresponds to the third vertical frequency (mode 5) of the Chacao Bridge. For higher order modes, which are not included in Table 6.3, larger differences of the frequencies are obtained, which lead to a reorder of the modes, as discussed later.

The modal contribution factors and the modal contribution to the base shear of the central pylon in the transverse and longitudinal direction are shown in Figure 6.3. The Figure shows the ten modes with larger $\overline{r}_n$ for each model with varying elastic modulus. For the base shear in the longitudinal direction, the mode with the largest static contribution in three cases is mode 10 ($\approx$0.199 Hz), which can be easily recognized in Figure 6.3 (c). The exception is the bridge with $0.75E_c$, in which the largest static contribution is provided by the mode 138. In the four cases, the largest contribution to the base shear in the longitudinal direction is given by the same mode (which is recognized by the mode shape). However, the frequency of this mode is different in the four cases as a consequence of the different of stiffness of the central pylon, as can be observed in Figure 6.3 (d).

To analyze the effect of the central pylon stiffness in the total base shear of the three pylons in the longitudinal and transverse directions, the modulus of elasticity of the central pylon is varied from $0.75E_c$ to $2.00E_c$ with increments of $0.05E_c$. For each case, the base shear is estimated with 500 modes and SRSS modal combination rule. The variation of the base shear of the three pylons are shown in Figure 6.4.

The base shear of the central pylon in the longitudinal direction (Figure 6.4 (a)) has an erratic behavior in the range 0.80 - 1.35 E_c, with no evident tendency. The average base shear in this range is 4.9%W, and the standard deviation is 0.6%W. Therefore, in this stiffness range a base shear of 4.9$\pm$ 0.6%W is estimated. Above $1.35E_c$, there is a tendency, and the base shear increases as E_c increases. In fact, the base shear increases 44% when the elastic modulus of the central pylon increases from $1.00E_c$ to $2.00E_c$. Figure 6.4 (b) shows that the base shear of the south and north pylon in the longitudinal direction is almost constant for the range 0.90-$1.15E_c$. For larger elastic modulus, these base shears increase as the stiffness of the central pylon increases. Finally, the base shear of the three pylons in the transverse directions are almost constant for an elastic modulus near $1.00E_c$.

The longitudinal displacement at the top of the central pylon is also calculated for the different values of the elastic modulus of the central pylon considering 500 modes. Figure 6.5 shows, as expected, that the displacement decreases as the elastic modulus increases.

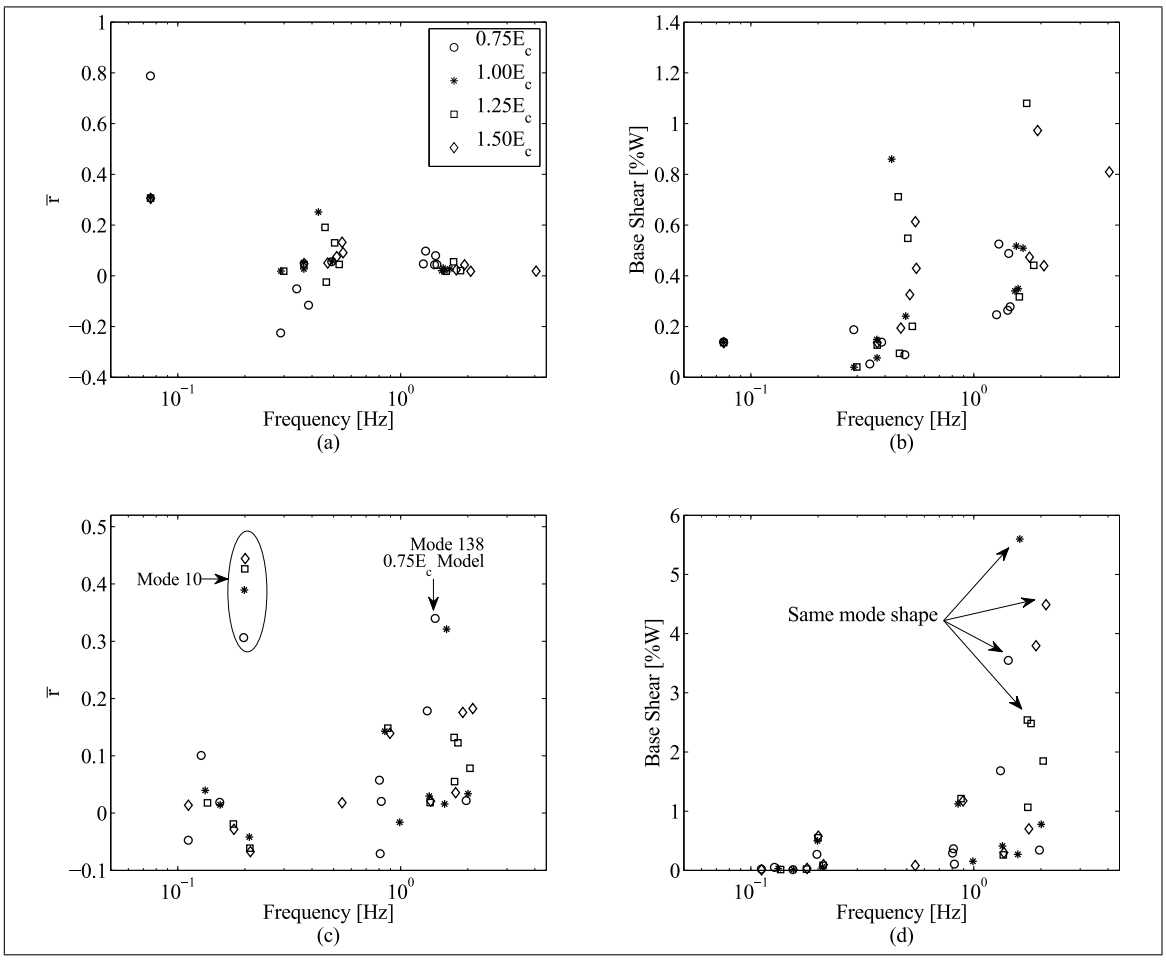

Figure 6.3. Modal contribution factors and modal base shear of the ten predominant modes for different values of E_c. (a) Modal contribution factors in the transverse direction, (b) Modal contribution to the base shear in the transverse direction, (c) modal contribution factors in the longitudinal direction and (d), modal contribution to the base shear in the longitudinal direction

For $0.90E_c$, a reduced displacement of 6.3 cm is observed, which agree with the reduced base shear of 4.1%W in the longitudinal direction of the central pylon (Figure 6.4).

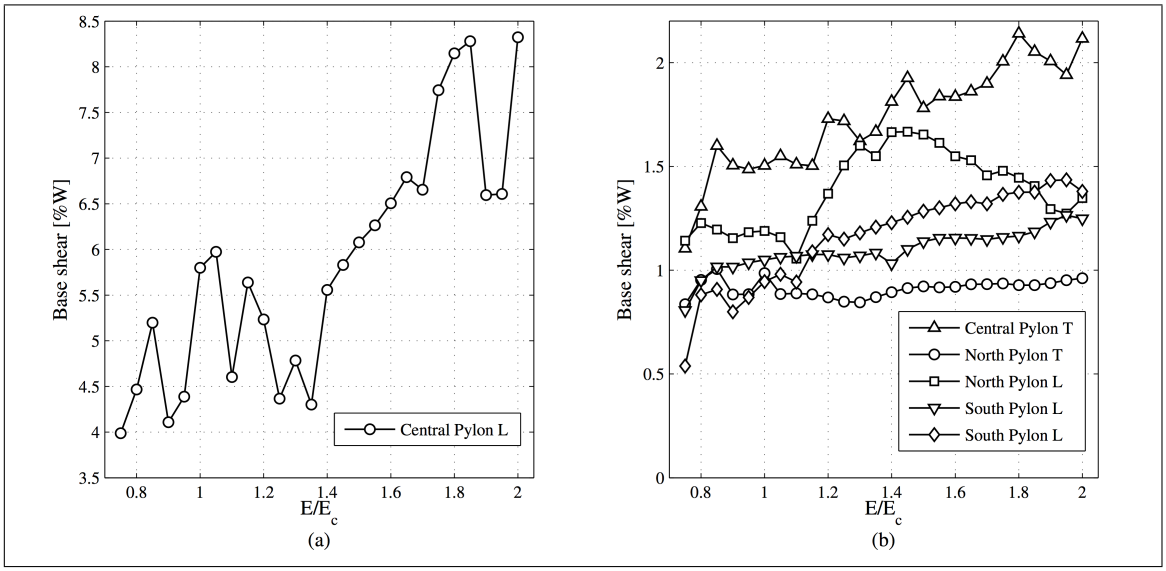

Figure 6.4. Base shear of the pylons for varying elastic modulus of the material of the central pylon. (a) central pylon in the longitudinal direction, (b) other cases

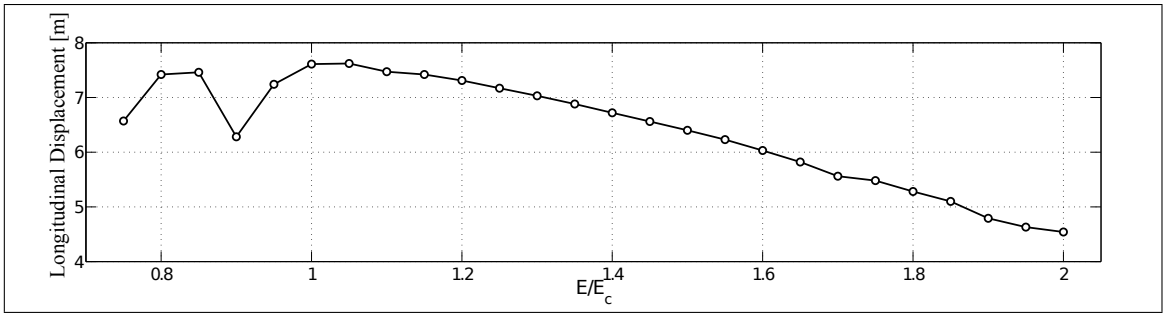

Figure 6.5. Longitudinal displacement at the top of the central pylon

7. CONCLUSIONS

This paper presents a study of the dynamic characteristics of a longitudinally asymmetrical multi-span suspension bridge. The study case is the current design of the Chacao Bridge (as of March 2015), that will be constructed by 2020 in Chile. The main conclusions can be summarized as follows:

- The Chacao Bridge will have two main spans of 1,055 m and 1,155 m and will be the longest multi-span suspension bridge in the world and the first one with a longitudinal asymmetry configuration.
- To study the dynamic characteristics of the current design of the Chacao Bridge a three dimensional finite element model was developed. To obtain the initial tension of the main cables in the finite element model, an initial static analysis with the dead load was conducted.
- Results showed that the first two modes corresponds to transverse vibrations of the deck with frequencies of 0.0625 Hz and 0.0755 Hz. The third and fourth mode correspond to vertical vibrations, with frequencies of 0.1115 Hz and 0.1205 Hz, respectively.
- The obtained lateral frequencies and mode shapes of the asymmetric Chacao Bridge are similar than those of the symmetric Taizhou Bridge. However, the vertical modes shapes of these bridges are different because independent vibrations of the main spans were observed in some modes of the Chacao Bridge.
- The contribution of the modes to the seismic base shear of the three pylons was identified. 40 modes are required to obtain a modal static contribution larger than 0.95 for the base shear in the transverse direction of the three pylons, and just 15 modes are required for the base shear in the longitudinal direction. For the base shear of the central pylon in the longitudinal direction, the base shear can be estimated with negligible error (3.7%) with only one mode (mode 151). This mode should be used to conduct a pushover analysis of the central pylon in the longitudinal direction of the bridge.

- From the parametric analysis of the central clamps it is concluded that in a longitudinally asymmetric multi-span suspension bridges four distribution cases of central clamps must be analyzed, and the election should be done considering that a reduction in the base shear of a particular direction of a central pylon can increase the base shear of others. For example, when central clamps are provided in both spans, the seismic base shear of the central pylon in the longitudinal direction decreases 30%, but the base shear in the transverse direction increases 20%.
- From the parametric study of the stiffness of the central pylon, it is concluded that it stiffness does not affect the low frequency transverse modes. However, it stiffness affects the vertical and longitudinal modes, with exception of the first two vertical modes. The base shear in the longitudinal direction of the central pylon increases when the stiffness of the pylon increases, but large variations of the base shear were observed for an elastic modulus of the central pylon in the range of 0.8 - 1.35 E_c.

7.1. Future Works

There are some modeling aspects that were not included in this study. An extension of this work consist in doing time-history analysis of the Chacao Bridge considering the non-linear behavior of the cables. This will give a more accurate response of the bridge under seismic action. It is also proposed to do the same analysis but considering different ground motions in the three pylons, because they are separated by long distances and in different local conditions. Moreover, a shake table study of the complete bridge can be done.

In this study the influence of the central clamps and the stiffness of the central pylon was analyzed, but there are more elements that can be relevant in the behavior of the bridge. The seismic, static and aerodynamic behavior of the bridge can be study by varying the sag of the main cables, the elevation of the deck from the sea, and the side span. The

last element can be deeply studied by considering different configurations of the bridge: with side span in the north side (like the current design), with side span in the south side, side span in both sides and no side spans.

The Chacao Bridge has other interesting topics outside the seismic area. A flutter stability analysis can be made in the bridge to analyze the effect of its longitudinally asymmetry. The ship impact on the pylons and the deck can also be studied. About the main cables, an important study is to find the initial shape of them and propose a constructive sequence of the deck.

Finally, when the Chacao Bridge is complete, a system identification can be done. With this data, the finite element model developed in this thesis can be verified and updated for more accurate results.

REFERENCES

Abdel-Ghafar, A., & Rubin, L. (1983). Vertical seismic behaviour of suspension bridges. *Earthquake Engineering and Structural Dynamics*, *1*(11), 1-19.

Abdel-Ghaffar, A., & Nazmy, A. (1991). 3D nonlinear seismic behavior of cable-stayed bridges. *Journal of Structural Engineering*, *117*(11), 3456-3476.

Abdel-Rohman, M. (2010). The influence of the higher order modes on the dynamic response of suspension bridges. *Journal of Vibration and Control*, *9*(18), 1380-1405.

Ali, H. M., & Abdel-Ghaffar, A. M. (1995). Modeling the nonlinear seismic behavior of cable-stayed bridges with passive control bearings. *Computers and Structures*, *54*(3), 461-492.

Angermann, D., Klotz, J., & Reigber, C. (1999). Space-geodetic estimation of the Nazca - South American vector. *Earth and Planetary Science Letters*, *171*(3), 329-334.

ANSYS® Academic Research, Release 15.0. (2013). *Help System, ANSYS Mechanical APDL Element Reference*. ANSYS, Inc.

Chopra, A. (2012). *Dynamics of structures*. Prentice Hall.

Ernst, H. (1965). Der e-modul von seilen unter berücksichtigung des durchhanges. *Der Bauingenieur*, *40*(2), 52-55.

Forsberg, T. (2001). Multi-span suspension bridges. *International Journal of Steel Structures*, *1*(1), 63-73.

Fukuda, T. (1967). Analysis of multi-span suspension bridges. *Journal of Structural Division*, *1*(1), 63-73.

Fukuda, T. (1968). Multi-span suspension bridges under lateral loads. *Journal of Structural Division*, *94*(ST1), 133-152.

Fukuda, T. (1975). Multi-span suspension bridges under torsional loads. *Journal of Japan Society Engineering*, *24*(2), 91-103.

Ge, Y., & Xiang, H. (2011). Extension of bridging capacity of cable-supported bridges

using double main spans or twin parallel decks. *Structure and Infrastructure Engineering: Maintenance, Management, Life-Cycle Design and Performance*, *7*(7-8), 551-567.

Gimsing, N., & Georgakis, C. (2012). *Cable supported bridges: concept and design*. John Wiley & Sons.

Grimes, R., Lewis, J., & Simon, H. (1994). A shift block lanczos algorithm for solving sparse symmetric generalized eigen-problems. *SIAM Journal Matrix Analysis A*, *15*(1), 228-272.

Irvine, H. (1980). The estimation of earthquake-generated additional tension in a suspension bridge cable. *Earthquake Engineering and Structural Dynamics*, *3*(8), 267-273.

Irvine, M. (1981). *Cable structures*. MIT Press.

Karoumi, R. (1999). Some modeling aspects in the nonlinear finite element analysis of cable supported bridges. *Computers and Structures*, *71*(4), 397-412.

Kim, K. S., & Lee, H. S. (2001). Analysis of target configurations under dead loads for cable-supported bridges. *Computers and Structures*, *79*(29), 2681-2692.

Larsen, A. (1993). Aerodynamic aspects of the final design of the 1624 m suspension bridge across the Great Belt. *Journal of Wind Engineering and Industrial Aerodynamics*, *48*(2-3), 261-285.

Li, J., Yan, J., Peng, T., & Han, L. (2014). Shake table studies of seismic structural systems of a Taizhou Changjiang Highway Bridge Model. *Journal of Bridge Engineering*.

Meriam, J., & Kraige, L. (2006). *Statics*. John Wiley & Sons.

MOP. (2001). *Chacao bridge, basic engineering studies, seismic hazard*.

Nazir, C. (1986). Multi-span balanced suspension bridges. *Journal of Structural Engineering*, *112*(11), 2512-2527.

Qiang, Z., He-qiang, T., & Guang-wu, Y. (2012). Selection of a structural system for a three tower suspension bridge of Maanshan Yangtze River Highway Bridge. *Structural Engineering International*, *22*(1), 139-143.

Ren, W., Blandford, G., & Harik, I. (2004). Roebling Suspension Bridge. I: Finite-element

model and free vibration response. *Journal of Bridge Engineering*, *9*(2), 110-118.

Sato, K. (1971). Deflection theory of multi-span suspension bridges considering deflection of towers and its numeral examples of various influence lines. *Proceedings of Japan Society Civil Engineering*, *190*(11-21).

Siringoringo, D., & Fujino, Y. (2008). System identification applied to long-span cable-supported bridges using seismic records. *Earthquake Engineering and Structural Dynamics*, *3*(37), 361-386.

Tada, K., Jin, H., Kitagawa, M., Nitta, A., & Toriumi, R. (1995). Effect of the Southern Hyogo Earthquake on the Akahi-Kaikyo Bridge. *Structural Engineering International*, *5*(3), 179-181.

Thai, H., & Choi, D. (2013). Advanced analysis of multi-span bridges. *Journal of Constructional Steel Research*, *90*, 29-41.

Thai, T., & Seung-Eock, K. (2011). Nonlinear static and dynamic analysis of cable structures. *Finite Elements in Analysis and Design*, *47*(3), 237-246.

Valenzuela, M., & Marquez, M. (2014a). Chacao Suspension Bridge: Special structural singularities. In *Proceeding of the 1 international bridges conference: Future challenges: design, construction and maintenance.*

Valenzuela, M., & Marquez, M. (2014b). Chacao Suspension Bridge: tender and technical callenges. In *Proceedings of the 37th IABSE symposium: Engineering for progress, nature and people.*

Wang, H., Tianyou, T., Hua, X., & Ahsna, K. (2014). Parameter sensitivity on flutter stability of a long-span triple-tower suspension bridge. *Journal of Wind Engineering and Industrial Aerodynamics*, *128*, 12-21.

Wang, H., Zou, K., Li, A., & Jiao, C. (2010). Parameter effects on the dynamic characteristics of a super-long-span triple-tower suspension bridge. *Journal of Zhejiang University-SCIENCE A*, *11*(5), 305-316.

Xu, Y., Ko, J., & Zhang, W. (1997). Vibration studies of Tsing Ma suspension bridge. *Journal of Bridge Engineering*, *2*(4), 149-156.

Yoshida, O., Okuda, M., & Moriya, T. (2004). Structural characteristics and applicability

of four-span suspension bridge. *Journal of Bridge Engineering*, *9*(5), 453-463.

Zhang, A., & Ge, Y. (2014). Flutter mode transition of a double-main-span suspension bridge in full aeroelastic model testing. *Journal of Bridge Engineering*, *19*(7), 06014004.